

DESIGN AND MANUFACTURING OF A SOLAR POWERED UNMANNED
AIR VEHICLE

A THESIS SUBMITTED TO
THE GRADUATE SCHOOL OF NATURAL AND APPLIED SCIENCES
OF
MIDDLE EAST TECHNICAL UNIVERSITY

BY

SERVET GÜÇLÜ ÖZCAN

IN PARTIAL FULFILLMENT OF THE REQUIREMENTS
FOR
THE DEGREE OF MASTER OF SCIENCE
IN
AEROSPACE ENGINEERING

DECEMBER 2015

Approval of the thesis:

**DESIGN AND MANUFACTURING OF A SOLAR POWERED UNMANNED AIR
VEHICLE**

submitted by **SERVET GÜÇLÜ ÖZCAN** in partial fulfillment of the requirements for
the degree of **Master of Science in Aerospace Engineering Department, Middle
East Technical University** by,

Prof. Dr. Gülbin Dural Ünver
Dean, Graduate School of **Natural and Applied Sciences**

Prof. Dr. Ozan Tekinalp
Head of Department, **Aerospace Engineering**

Prof. Dr. Nafiz Alemdaroğlu
Supervisor, **Aerospace Engineering Department, METU**

Examining Committee Members:

Prof. Dr. Altan Kayran
Aerospace Engineering Department, METU

Prof. Dr. Nafiz Alemdaroğlu
Aerospace Engineering Department, METU

Prof. Dr. Serkan Özgen
Aerospace Engineering Department, METU

Assist. Prof. Dr. Ali Türker Kutay
Aerospace Engineering Department, METU

Assist. Prof. Dr. Levent Ünlüsoy
Aeronautical Engineering, UTAA

Date:

I hereby declare that all information in this document has been obtained and presented in accordance with academic rules and ethical conduct. I also declare that, as required by these rules and conduct, I have fully cited and referenced all material and results that are not original to this work.

Name, Last Name: SERVET GÜÇLÜ ÖZCAN

Signature :

ABSTRACT

DESIGN AND MANUFACTURING OF A SOLAR POWERED UNMANNED AIR VEHICLE

Özcan, Servet Güçlü

M.S., Department of Aerospace Engineering

Supervisor : Prof. Dr. Nafiz Alemdaroğlu

December 2015, 76 pages

The aim of this thesis is to describe the conceptual design, performance analysis including solar energy collection and manufacturing process of a solar powered unmanned aerial vehicle (UAV) and validate the design through ground and flight tests. Through a literature survey of solar powered aircraft, main design requirements are chosen. The solar powered UAV designed for this study is a small scale aircraft and intended to be used simply and frequently by end-users. Therefore it is designed as a flying wing, to lower the cost of the manufacturing by simplifying the process. The manufacturing process is evaluated for further simplification and cost-effectiveness. For ease of production, the flying wing is cut out from EPP/EPS foam blocks by hot wire, as two wings and one blended center piece (fuselage). The reinforcing structures are embedded in these foam-cut parts and two transparent winglets are assembled to the wing tips. At this step, the flying wing made its maiden flight without the solar panels to verify the design. After the maiden flight, solar panels are embedded on to the wings and ground test is conducted to verify the estimations on the solar energy collection by these panels. Lastly, the solar flying wing is flown a second time to observe its performance including the solar panels.

Keywords: Solar powered UAV, flying wing design, solar array design, renewable

energy applications, solar energy

ÖZ

GÜNEŞ PANELLİ İNSANSIZ HAVA ARACI TASARIMI VE ÜRETİMİ

Özcan, Servet Güçlü

Yüksek Lisans, Havacılık ve Uzay Mühendisliği Bölümü

Tez Yöneticisi : Prof. Dr. Nafiz Alemdaroğlu

Aralık 2015 , 76 sayfa

Bu tezin amacı, güneş panelli bir insansız hava aracının (İHA) tasarımını, güneş enerjisi toplama performansını içeren performans analizlerini ve üretim aşamalarını anlatmak; bu aşamalar sonucunda prototip bir hava aracı üreterek, yer ve uçuş testleri ile bu hava aracının işlevselliğini doğrulamaktır. Bu amaç doğrultusunda öncelikle, güneş enerjisi ile uçan hava araçlarında yapılan literatür taraması ile temel tasarım gereksinimleri belirlenmiştir. Üretilecek İHA'nın küçük İHA sınıfında olması planlanmış, böylece son kullanıcı için basit ve sürekli kullanılabilen bir hava aracı olması hedeflenmiştir. Uçan kanat tasarımı ile üretim aşamalarını basitleştirilmiş ve maliyeti düşürülmüştür. Aynı zamanda üretim yöntemleri de incelenerek, bu aşamalarda daha da iyileştirilme yapılmasına çalışılmıştır.

Üretim kolaylığı açısından, uçağın kanat ve birleştirilmiş gövde parçalarının EPP-/EPS köpükten sıcak tel ile kesilip çıkarılmasına karar verilmiştir. Diğer iç yapısal elemanlar bu köpükten parçalara gömülmüş, pleksi-glastan kesilmiş iki şeffaf uç kanat da kanatların ucuna eklenmiştir. Bu ilk üretim aşamasından sonra prototip uçak, üzerinde güneş hücreleri olmadan ilk uçuşunu yaparak tasarımı ve performansı doğrulanmıştır. Bu uçuştan sonra, kanatlar üzerine güneş hücreleri yerleştirilerek yer testi ile hesaplanan güneş enerjisi toplama değerleri doğrulanmıştır. Son olarak da, prototip hava aracı tekrar uçurularak güneş hücreleri ile genel performansı değerlendirilmiştir.

Anahtar Kelimeler: Güneş panelli İHA, uçan kanat tasarımı, güneş paneli tasarımı, yenilenebilir enerji uygulamaları, güneş enerjisi

*To my newly enlarged family, my Sena, my two grandfathers who inherited me the
joy of aviation and joy of life..*

ACKNOWLEDGMENTS

I would like to thank my supervisor Prof. Nafiz ALEMDAROĞLU for his constant guidance, friendship and his trust in me. It was a great honor to work with him for the last four years and I hope our cooperation will continue in the future.

I am very grateful to all people I know during my graduate studies in METU-AEE, they completed me and changed me deeply in points of life, experience and friendship. I am very lucky to be included in the group "Havacı Tayfa". I would also like to thank my fiancée Sena YAZIRLI for her never-ending love, patience and support and changing my world to a true heaven on Earth.

I would also like to thank my manager and colleagues in ASELSAN who provided me every means they and the company can possibly offer to make production and testing of this thesis work possible.

Lastly and most deeply, sincerest thanks to each of my family members, my father Dođan ÖZCAN who runs the aviator's blood in the family; my mother Aysel ÖZCAN whom I got 99% of my genes from; and my older sister and brother-in-law Güneş and Sabri BURCU for being closest to me. They always supported me in every way and believed in me all the way through my life.

TABLE OF CONTENTS

ABSTRACT	v
ÖZ	vii
ACKNOWLEDGMENTS	x
TABLE OF CONTENTS	xi
LIST OF TABLES	xiv
LIST OF FIGURES	xv
CHAPTERS	
1 INTRODUCTION	1
1.1 A BRIEF HISTORY OF SOLAR POWER AND SOLAR AVIATION	1
1.2 DESIGN APPROACH AND OBJECTIVE	4
2 CONCEPTUAL DESIGN AND PERFORMANCE ANALYSIS	7
2.1 BASIC CONCEPTS ABOUT FLYING WINGS	7
2.1.1 AIRFOILS FOR FLYING WINGS	7
2.1.2 NEUTRAL POINT AND STABILITY OF SWEPT FLYING WINGS	10
2.1.3 TWIST	12

2.2	BASIC CONCEPTS ABOUT SOLAR ENERGY AND SOLAR CELLS	12
2.2.1	SOLAR ENERGY AND SOLAR IRRADIANCE .	12
2.2.2	SOLAR CELLS	13
2.3	CONCEPTUAL DESIGN	17
2.3.1	INITIAL SIZING	17
2.4	PERFORMANCE ANALYSIS	24
2.4.1	WING LOADING	24
2.4.2	POWER AVAILABLE AND POWER REQUIRED CURVES	24
2.4.3	RATE OF CLIMB AND TIME OF CLIMB	29
2.5	DESIGN OUTPUTS AND 3-D MODEL	29
2.6	MATERIAL SELECTION	32
3	MANUFACTURING	33
3.1	PRODUCTION OF MAIN PARTS	33
3.2	INTEGRATION OF STRUCTURAL ELEMENTS	37
3.2.1	PRODUCTION OF STRUCTURAL ELEMENTS	37
3.2.2	INTEGRATION TO WING PIECE 2	40
3.2.3	INTEGRATION TO WING PIECE 1	42
3.2.4	INTEGRATION TO FUSELAGE	44
3.3	INTEGRATION OF AVIONICS	48
3.4	OVERALL REVIEW AND ASSEMBLY	50

3.5	PRODUCTION OF SOLAR CELLS AND CHARGING CIR- CUIT	52
4	GROUND AND FINAL FLIGHT TESTING	57
4.1	GROUND TESTS	57
4.2	MAIDEN FLIGHT TEST	68
5	CONCLUSION	73
	REFERENCES	75

LIST OF TABLES

TABLES

Table 1.1	Solar Powered Aircraft	3
Table 1.2	Solar Powered Aircraft (continued)	4
Table 2.1	Comparison of stabilities of conventional and reflexed airfoils [3] . .	9
Table 2.2	Moment coefficient and zero lift angle data of E 186 and MH 61 airfoils	20
Table 2.3	Required inputs found after iterations and calculations	21
Table 2.4	Chosen solar cell properties	28
Table 2.5	Design parameters	30
Table 2.6	Estimated Weight Distribution	31

LIST OF FIGURES

FIGURES

Figure 2.1	Geometric representation of the location of NP [3]	11
Figure 2.2	Spectrum of solar radiation [14]	13
Figure 2.3	Main components of a solar cell	14
Figure 2.4	Solar cell working principles	14
Figure 2.5	History of Cell Efficiencies [6]	16
Figure 2.6	E 186 airfoil [11]	18
Figure 2.7	MH 61 airfoil [12]	18
Figure 2.8	Polar curves of E 186 [11]	19
Figure 2.9	Polar curves of MH 61 [12]	20
Figure 2.10	Graph of β_{req}^* vs AR for different $\phi_{0.25}$ and the equation to calculate β_{req}^* [3]	22
Figure 2.11	Graph of β_{cm}^* vs AR for different $\phi_{0.25}$ and the equation to calculate β_{cm}^* [3]	23
Figure 2.12	Power system of solar powered UAV [5]	25
Figure 2.13	Power vs velocity curves	29
Figure 2.14	Fully assembled UAV	30
Figure 2.15	Front, top, ISO and side views of the solar powered UAV design . .	31
Figure 3.1	Main parts of the UAV	34
Figure 3.2	Production of Wing Piece 1 and 2 in hot wire CNC foam cutter . .	34
Figure 3.3	Surface quality check for produced part	35
Figure 3.4	Production of fuselage and the produced part	35

Figure 3.5	Weights of foam parts	36
Figure 3.6	Production of Rectangular Composite Spars	37
Figure 3.7	Lengths and positions of connection spars with respect to rectangular spars and end ribs	38
Figure 3.8	Production of Connection Rods	38
Figure 3.9	Templates for the end ribs with the positions of connection and main spars	39
Figure 3.10	Production of 1.5 mm carbon fiber plate end ribs	39
Figure 3.11	Gluing of the end ribs and drawing the control surface and rear spar location	40
Figure 3.12	Gluing of rear spar and control surface production	40
Figure 3.13	Drawing locations for rectangular spars and their integration into the part	41
Figure 3.14	Drawing guide lines, shaping one side of the spar as teeth and integration of spars	41
Figure 3.15	Gluing of the end ribs and drawing the spar locations	42
Figure 3.16	Integration of rectangular spars into the part	42
Figure 3.17	Burying of the 10 mm spars into Wing Piece 1	43
Figure 3.18	Checking the fitting of two pieces together	43
Figure 3.19	Trimming of fuselage leading edge for blending the shape to wings	44
Figure 3.20	Gluing of end ribs to the fuselage and integration of main spars	44
Figure 3.21	Checking the fitting of connection spars of Wing Piece 1 to fuselage	45
Figure 3.22	Manufacturing of engine mount area	45
Figure 3.23	Metal motor mount piece assembly	46
Figure 3.24	Drawing guidelines for rooms and formation of these rooms inside fuselage	46
Figure 3.25	Production of composite layers for upper and lower surfaces of the fuselage	47
Figure 3.26	Upper and lower surfaces of the manufactured fuselage	47

Figure 3.27 Avionics and their weight	49
Figure 3.28 Servo integration to Wing Piece 1	49
Figure 3.29 Assembly of motor to its mount	50
Figure 3.30 Progress of the UAV from the first foam parts to the ready-to-fly final version	51
Figure 3.31 Isometric views of the UAV	52
Figure 3.32 Calculations done for solar cell placement over Wing Piece 1	53
Figure 3.33 Making templates from the upper surface molds of each part	54
Figure 3.34 Making templates from the upper surface molds of each part	55
Figure 3.35 Soldering the cells in series	55
Figure 3.36 90 solar cell group that will be tested and will be part of the solar cell grid on the UAV	56
Figure 4.1 Motor Thrust Test setup	58
Figure 4.2 Current, voltage and power readings at required thrust for cruise, as an example	58
Figure 4.3 ESC Data of the Motor Thrust Test	59
Figure 4.4 Current vs. Thrust graph of the motor test	60
Figure 4.5 Schottky diodes (black) soldered at the positive pole of the solar cell groups	61
Figure 4.6 A view of the clearness of the sky on the test day	61
Figure 4.7 Test setup (left) and the voltage reading from the 90-cell group (right)	62
Figure 4.8 Test setup with the battery only	63
Figure 4.9 Test setup with battery, MPPT and solar cells	64
Figure 4.10 Consumption from the battery for only battery case (left) and con- sumption from the battery for battery, MPPT and solar cells case	64
Figure 4.11 ESC data graph of the test with the battery only	65
Figure 4.12 ESC data graph of the test with battery, MPPT and solar cells	66
Figure 4.13 Fully assembled UAV prototype ready for RC maiden flight	68

Figure 4.14 Hand-launch of the UAV (1); giving full throttle command (2); UAV rolls left uncontrollably (3); UAV crash-lands on its left side	69
Figure 4.15 Application of Carbon fiber and E-glass fiber to the lower side of Wing Piece 2 of both wings	70
Figure 4.16 Addition of Carbon layer and adhesive to root spars of the wings . .	70
Figure 4.17 Hand-launch (1); take-off (2); climb (3) and flight (4) of the UAV during its maiden flight	71
Figure 4.18 UAV landed after its maiden flight	72
Figure 4.19 The solar powered UAV with solar cells on its wings, before fixing	72

CHAPTER 1

INTRODUCTION

1.1 A BRIEF HISTORY OF SOLAR POWER AND SOLAR AVIATION

The Sun has always been the ultimate energy source for life on Earth, through photosynthesis process in plants. Humans may not be able to convert Sun's incoming energy directly to any products by biological means. They recognized it in very early ages of civilization: by simply making fires using simple magnifying glasses since 7th century B.C. From that time on, Sun's thermal energy is harnessed by humans for mainly heating and burning purposes. At the beginning of the 19th century, scientists like Robert Stirling started working on heat engines that uses this thermal energy to produce mechanical power. These engines and the theory behind them are predecessors of solar dish collector power plants today. These power plants use the thermal energy from the Sun to produce electrical energy by means of steam turbines. It is a clean and efficient way of producing electricity from Sun light but it is still not a direct method.

It was not until 1876 that the first steps of photovoltaics are taken. Photovoltaics is the method of turning light energy directly into electrical energy by means of exciting and emitting electrons in semiconductor material, which is called "the photoelectric effect" in physics. In 1876, William Grylls Adams and Richard Evans Day discovered that selenium produces electricity when exposed to light. Although selenium solar cells failed to convert enough sunlight to power electrical equipment, they proved that a solid material could change light into electricity without heat or moving parts [7]. The research on the theory and the semiconductor materials continued and in 1954 first photovoltaic cells were developed at Bell Laboratories by Daryl Chapin,

Calvin Fuller, and Gerald Pearson. These silicon cells had 4% conversion efficiency but they were quickly increased to 11% efficiency later that year [8]. After 1958, photovoltaic cells were started to be used on satellites to power their equipment in space. Today the main electrical power source for almost every satellite is solar energy [10]. Photovoltaic cells started to descend from space to Earth's surface and atmosphere in 1970's, when Dr. Elliot Berman, with help from Exxon Corporation, designed a significantly less costly solar cell, bringing price down from \$100 per Watt to \$20 per Watt. With this significant drop in the costs, solar cells begin to be used commercially like for navigation warning lights and horns on offshore gas and oil rigs, lighthouses, railroad crossings. Domestic solar applications in remote locations began to be feasible where grid-connection can cost too much [9]. This also triggered the start of solar aviation at the end of 1974 with Sunrise I, designed by R.J. Boucher from Astro Flight Inc. under a contract with ARPA. This model airplane had a wingspan of 9.76 m and weighed 12.25 kg. It flew for 20 minutes at an altitude of 100 m in at Camp Irwin, California. Almost simultaneously and without the knowledge of these tests taking place in the USA, Helmus Bruss was working on a solar model airplane in Germany in 1975. He and his friend Fred Militky, who was also a great pioneer in electric powered flight with model aircraft, achieved their first successful solar flight with Solaris in 1976, with 150 seconds of flight duration at an altitude of 50 m [4]. The solar aviation became more and more popular in 40 years after its first steps, with each achievement in solar cell conversion efficiency and cost reduction. Many aircraft were built, both manned and unmanned, with the purpose of using the solar energy for unlimited flight. Unmanned aircraft are more popular today, as unlimited flight requires eliminating the human factor on board whose endurance and environmental tolerance is limited. The list of successful aircrafts built is shown in Table 1.1 and 1.2 below.






Aircraft Name	MTOW (kg)	Wingspan (m)	Endurance (hours)	Range (km)	Cruise Speed (km/h)	Max. Ceiling (m)	Photograph
(Unmanned) Sunrise I	12.3	9.8	0.3	-	-	100	
(Unmanned) Sunrise II 1975	10.2	9.8	0.4	-	-	100	
(Unmanned) Solaris 1976	1.0	-	0.04	-	-	50	
(Manned) Icare 2 1996	-	25.0	-	-	-	450	
(Unmanned) Pathfinder 1998	254.0	30.0	-	-	-	15392	
(Unmanned) Solar Solitude 1996	2.0	2.7	-	38.8	-	1283	
(Unmanned) Solar Excel 1990	0.7	2.1	11.5	190.0	62.0	2065	

Table 1.1: Solar Powered Aircrafts







Aircraft Name	MTOW (kg)	Wingspan (m)	Endurance (hours)	Range (km)	Cruise Speed (km/h)	Max. Ceiling (m)	Photograph
(Manned) Solar Challenger 1981	-	14.2	5.5	262.0	-	-	
(Manned) SunSeeker 1990	1.9	-	6.0	400.0	-	-	
(Unmanned) Helios 1999-2003	-	70.0	24 (first overnight flight)	Unlimited	-	30000	
(Unmanned) SoLong 2005	11.5	4.8	48.0	Unlimited	-	-	
(Unmanned) Zephyr 2005	27.0	12.0	336.5	Unlimited	-	21562	
(Manned) Solar Impulse 2009	2000	80	Unlimited (First trip around the world)	Unlimited	-	-	
(Unmanned) Sky-Sailor 2004	2.4	3.2	27	Unlimited	-	-	

Table 1.2: Solar Powered Aircrafts (continued)

The design motivation of this thesis work comes from these solar powered aircraft, to stay aloft as long as possible using only clean and natural energy of the Sun.

1.2 DESIGN APPROACH AND OBJECTIVE

The design process of an aircraft involves three main phases:

- *Conceptual Design Phase*: the phase where main design requirements are guides to determine the sizing, weight estimation and general performance of the aircraft. This phase is not in too much detail but gives a good overall visualization of the aircraft.
- *Preliminary Design Phase*: the phase where aerodynamic, structural, control and propulsion system analyses are done. If significant changes to the overall geometry of the design should be made, the design process is restarted with the previous phase.
- *Detail Design Phase*: this is the final phase of the design where every detail on the aircraft are revisited and determined from both designer's and manufacturer's points of view, so that the prototype aircraft that will be built is both good and cheap enough to meet the initial requirements.

In this thesis, the last two phases are merged as they require iterative approach with the addition of the complexity of panel placement and solar energy collection management on the UAV. All of these phases will be explained and validated through flight and ground testing rather than computer aided analyses.

The main objective for this thesis is to design and manufacture a mini UAV which has extended endurance by using solar power. The UAV should be in mini class, so that it is easy to manufacture and can be widely used for commercial purposes. For extended endurance, the UAV should have the following properties:

- High aspect ratio, for low cruise speeds and better gliding performance
- High aerodynamic design, for low drag values
- Large wing area, for high solar energy collection

Considering these three important requirements, conventional aircraft with high aspect ratio wings and tails and very thin fuselage were designed and built as solar powered aircraft. However the drag can be lowered by a better aerodynamic design and slightly increasing the useful surface area for solar energy collection. Therefore, the design approach for this thesis work is to build a flying wing. This type of aircraft is a good choice as it has no surfaces or parts other than wings with large surface

area. Its central piece is a blended-wing body with significant volume for carrying instruments and payload. Having no other surfaces or parts significantly reduces the drag as well as ease of manufacturing. These properties of a flying wing design make it very suitable for a solar powered aircraft.

CHAPTER 2

CONCEPTUAL DESIGN AND PERFORMANCE ANALYSIS

2.1 BASIC CONCEPTS ABOUT FLYING WINGS

A flying wing is a tailless fixed-wing aircraft that has no definite fuselage. The crew, payload, fuel, and equipment are typically housed inside the main wing structure. Similar aircraft designs like blended wing body aircraft and micro-light aircraft are sometimes referred to as such [13].

A clean flying wing is sometimes presented as theoretically the most aerodynamically efficient (lowest drag) design configuration for a fixed wing aircraft. It also would offer high structural efficiency for a given wing depth, leading to light weight and high fuel efficiency [13]. These show again that this type of aircraft is very suitable to be made as solar powered where energy collection and spending is an important issue. On the other hand, as it does not have conventional stabilizing surfaces such as horizontal and vertical tails, the flying wing in its purest form can be unstable and difficult to control. The longitudinal stability issue is important to focus on while designing such an aircraft. This makes the design of a flying wing slightly complex but a suitable airfoil selection with a good combination of wing sweep and twist at the tips can solve the problems about stability.

2.1.1 AIRFOILS FOR FLYING WINGS

Flying wings can be equipped with almost any airfoil, if a good sweep and twist combination is chosen for the airfoil used. However, if the flying wing is to be designed for a wide operating range, the wing tips should have very small amount of twist

only, or none, to keep the induced drag at reasonable levels, so that the advantages of the flying wing design will not vanish. For this, moment coefficient variation of the wings should not vary too much as the angle of attack changes. This reason tightens the search of airfoils suitable for flying wings and constricts to choose low moment coefficient airfoils or even ones with positive moment coefficients. This class of airfoils is called “reflex airfoils”. A reflex airfoil’s trailing edge is upwards instead of downwards as in many other conventional airfoils. These airfoils create natural longitudinal stability due to their reflexed (s-shaped) camber lines.

In order to describe why reflex airfoils provide longitudinal stability, we need to focus on two important things:

- *Total Aerodynamic Forces and Moments*: the forces created by the difference in air pressures due to flow of air. These can be reduced to one total force and one total moment to act at the quarter-chord point ($c/4$) of the airfoil. This point is also the neutral point (NP) for unswept (plank) wings.
- *Center of Gravity (c.g.)* : the point at which total of the gravitational force, its total mass (m) times gravitational acceleration (g) of the aircraft acts on.

Considering these two locations and forces, we can easily compare the conventional airfoil with a reflex airfoil for the trimmed flight condition, where the aircraft is in equilibrium. Taking lift force (L) and its moment (M) and weight (mg) into consideration, the comparison of two different types of airfoils are explained briefly by Martin Hepperle in the Table 2.1 below. The forces with asterisk (*) superscript show the forces for the trimmed condition.

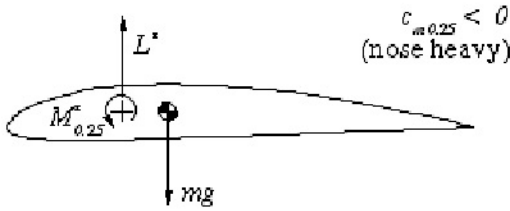
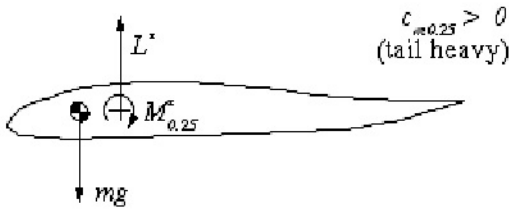
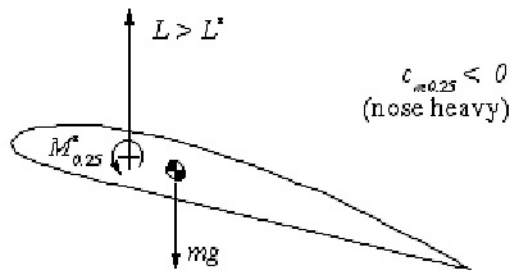
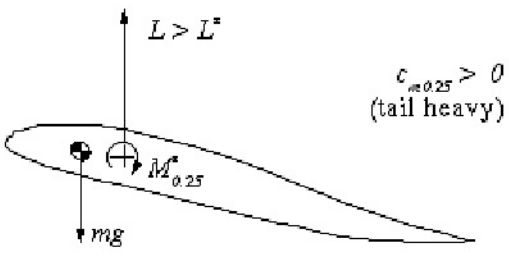
CONVENTIONAL AIRFOIL WITH CAMBER	AIRFOIL WITH REFLEXED MEAN LINE
EQUILIBRIUM STATE	
 <p style="text-align: right;">$c_{m0.25} < 0$ (nose heavy)</p>	 <p style="text-align: right;">$c_{m0.25} > 0$ (tail heavy)</p>
<p>This airfoil has a nose heavy moment. As stated above, the center of gravity is also the center of rotation of the wing. When it is shifted behind the $c/4$ point, the air force L^* in front of the $c.g.$ counteracts the nose heavy moment M^* to achieve equilibrium. The distance between $c.g.$ and $c/4$ point is depending on the amount of M^*. A symmetrical airfoil has $M^*=0$, which means we have to place the $c.g.$ at the $c/4$ point.</p>	<p>The reflexed camber line makes the moment coefficient positive, which means, that the moment around the $c/4$ point is working in the tail heavy direction. Therefore the center of gravity has to be located in front of the $c/4$ point to balance the moment M^* by the lift force L^*. The larger the moment (-coefficient) of the airfoil, the larger the distance between $c/4$ and the $c.g.$ for equilibrium.</p>
DISTURBED STATE	
 <p style="text-align: right;">$c_{m0.25} < 0$ (nose heavy)</p>	 <p style="text-align: right;">$c_{m0.25} > 0$ (tail heavy)</p>
<p>When the angle of attack is increased (e.g. by a gust), the lift force L increases. Now $L > L^*$ and the tail heavy moment due to the lift is larger than the moment around $c/4$, which still is $M=M^*$. Thus the wing will pitch up, increasing the angle of attack further. This behavior is instable and a tailplane is needed to stabilize the system.</p>	<p>Here, we have the air force acting behind the $c.g.$, which results in an additional nose heavy moment, when the lift increases. With $L > L^*$, the wing will pitch down, reducing the angle of attack, until the equilibrium state is reached again. The system is stable.</p>

Table 2.1: Comparison of stabilities of conventional and reflexed airfoils [3]

As seen in Table 2.1, reflex airfoils are suitable for sustaining longitudinal stability for flying wings. While they are being used, it is important to make sure that c.g is in front of $c/4$ of the airfoil chord, which also corresponds to NP for unswept wings. It was mentioned before that reflex airfoils are required but may not be sufficient enough by themselves so in addition to the use of reflex airfoils, wing sweep and twist may also be required. From this point on the calculations and stability of the swept and tapered flying wings will be explained, as these design features will be used for the present prototype solar powered UAV.

2.1.2 NEUTRAL POINT AND STABILITY OF SWEPT FLYING WINGS

As we have seen in previous part that an unswept wing with a reflexed airfoil is able to stabilize if its c.g. is located in front of its NP. The distance between these two points and its ratio to the mean aerodynamic chord (MAC) length of the wing gives the stability coefficient (σ). This coefficient can be described as percentage. For flying wings, this coefficient is generally between 2% and 5%.

For this value to be calculated, the NP of the swept wing must be found. As NP of an unswept and untapered wing corresponds to the $c/4$ of the airfoil chord directly; whereas for the tapered swept wing, the geometry gets more complex and therefore several calculations must be done.

Following the steps from [3], firstly taper ratio (λ) and the MAC length (l_μ) are calculated using 2.1 and 2.2:

$$\lambda = \frac{l_t}{l_r} \quad (2.1)$$

$$l_\mu = \frac{2}{3} \frac{1 + \lambda + (\lambda)^2}{1 + \lambda} l_r \quad (2.2)$$

From this point on, two methods can be used to determine the location of NP:

1- Graphical Approach:

The spanwise location of the MAC (y) can be calculated using the wing span (b) value

by below equation 2.3.

$$y = \frac{b}{2} \frac{l_r - l(\mu)}{l_r - l_t} \quad (2.3)$$

When the MAC is drawn on the wing at y distance from the central line, the location of NP corresponds to the horizontal line that passes through $c/4$ of the MAC. The distance of NP to the nose of the aircraft is represented as x_N , and its geometric location of this value is shown in 2.1.

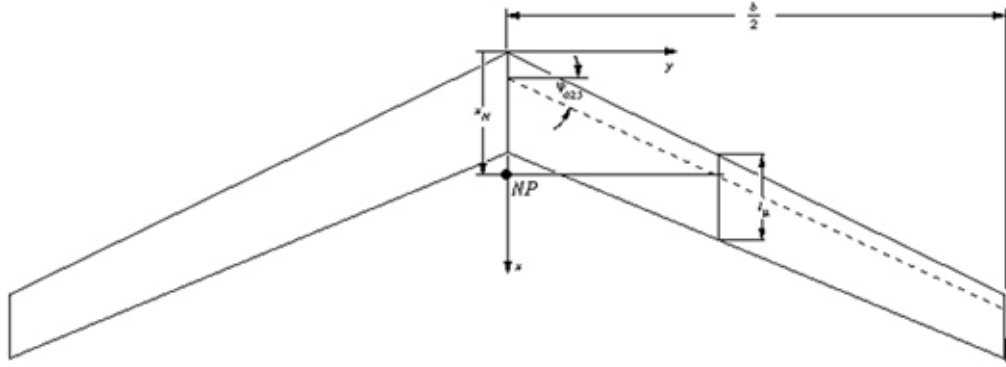


Figure 2.1: Geometric representation of the location of NP [3]

2- Specific Equations:

The location of NP from the nose of the aircraft (x_N) can also be calculated directly if the sweep angle from quarter chord ($\phi_{0.25}$) using Eqn (2.4) depending on the value of λ .

$$x_N = \begin{cases} \frac{l_r}{4} + \frac{2b}{3\pi} \tan \phi_{0.25} & \text{if } \lambda > 0.375 \\ \frac{l_r}{4} + \frac{b(1+2\lambda)}{6(1+\lambda)} \tan \phi_{0.25} & \text{if } \lambda < 0.375 \end{cases} \quad (2.4)$$

As the location of the NP and c.g. are determined along with the sweep angle of the wings, the required twist can be calculated.

2.1.3 TWIST

For conventional airplanes, it is possible to adjust the longitudinal stability and have the equilibrium of all the moments around c.g. with the help of the horizontal tail and elevator trimming during first flight tests. However for flying wings, there are no additional surfaces other than wings. Therefore the wing must be twisted towards the tip in order to achieve the equilibrium of all the moments around c.g. and eventually the longitudinal stability. Twist is the last requirement of the flying wing design and it is the only part that actually makes the design and manufacturing slightly complex. For the design part, the calculation of the twist depends on many parameters including root and tip airfoil parameters, sweep angle ($\phi_{0.25}$) and aspect ratio (AR). Mainly the required twist calculation is divided into two parts:

- *Geometric Twist* : This part is the applied twist to the wings, by creating an angle, equal to the required twist, between the chord lines of tip and root airfoils. If the tip airfoil is twisted downward w.r.t. the root airfoil then this is called a positive twist or a washout. This results in smaller angle of attack at the tip section.
- *Aerodynamic Twist* : This is done by selecting different airfoils for tip and root sections of the wings. If chosen specifically, the differences between the zero lift angles of these airfoils help reduce the required geometric twist. [3]

Explanation of the twist calculation will be done in the conceptual design part, as it is complex and need to be done for specifically for each aircraft.

2.2 BASIC CONCEPTS ABOUT SOLAR ENERGY AND SOLAR CELLS

2.2.1 SOLAR ENERGY AND SOLAR IRRADIANCE

The energy coming from the Sun is a grand total of the energies of photons with different wavelengths, which are present in the Sun's light rays. The wavelength spectrum of these photons is called the "solar spectrum" and it is given in Figure 2.2.

Spectrum of Solar Radiation (Earth)

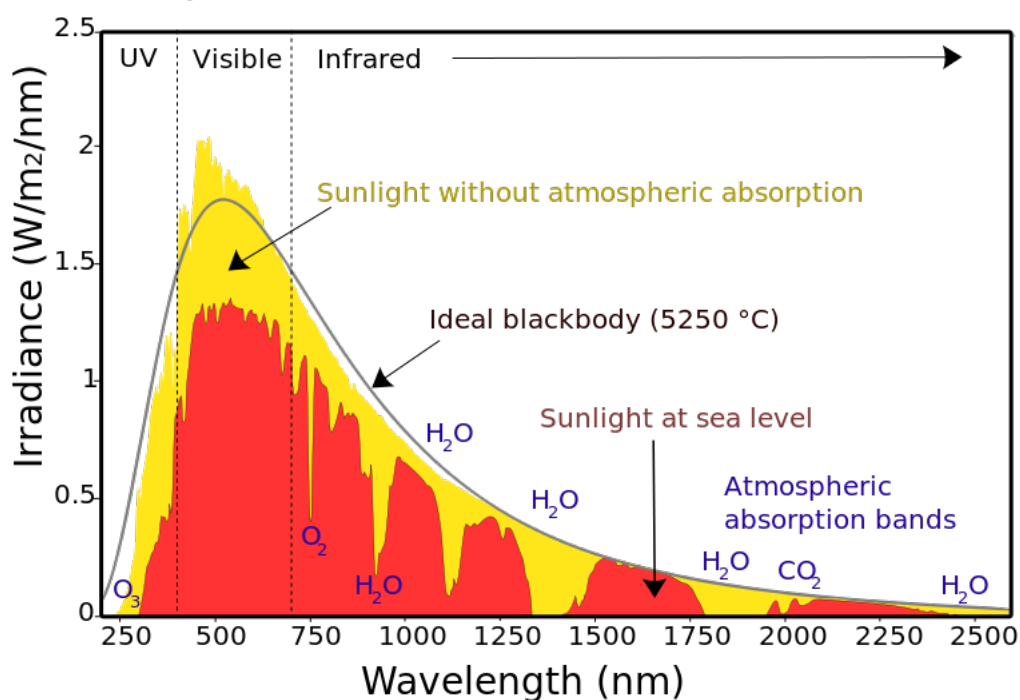


Figure 2.2: Spectrum of solar radiation [14]

The reference irradiance is for the measurements made just outside the atmosphere and therefore the sum of these energies corresponds to 1361 W/m^2 . This is a physical constant and it is called the Solar constant (G_{SC}). This value gets lower as the sunlight travels in the atmosphere, due to diffusion and absorption by clouds or other atmospheric elements. It gets down to 900 W/m^2 when it reaches the Earth's surface. The efficiency of a solar cell depends on how much it can convert the different light rays in this spectrum to electricity. The ideal solar cell theoretically can absorb all the wavelengths and its efficiency is 100%. Solar cells and their working principles will be explained briefly in the next part.

2.2.2 SOLAR CELLS

A solar cell or photovoltaic cell is a device that converts solar energy into electricity by the photovoltaic effect. It is a clean and long-duration source of energy requiring almost no maintenance. There are many types of solar cells which are composed of

various semiconducting materials, piled up on one or more layers. Silicon is especially used for production of solar cells as it is very easy to find and inexpensive. In this thesis, crystalline silicone (c-Si) panels will be used for low cost production. These cells are made of two layers of semiconductors, one with a high density of electrons (n-type) and the other with high density of electron acceptors (p-type) as shown in Figure 2.3.

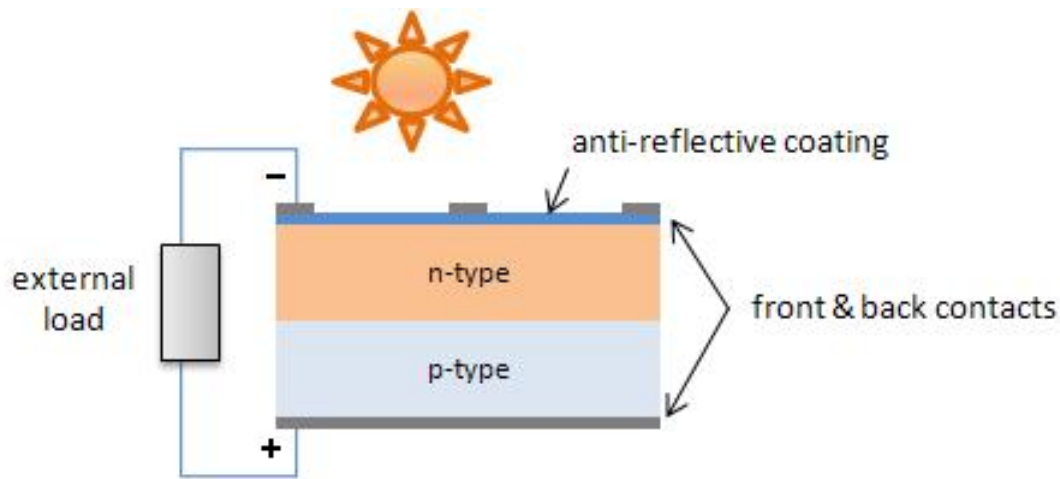


Figure 2.3: Main components of a solar cell

When sunlight hits the n-type plate, it gives enough energy to electrons to set free and by the help of a conductor these free electrons can move down to the p-type plate, as shown in Figure 2.4.

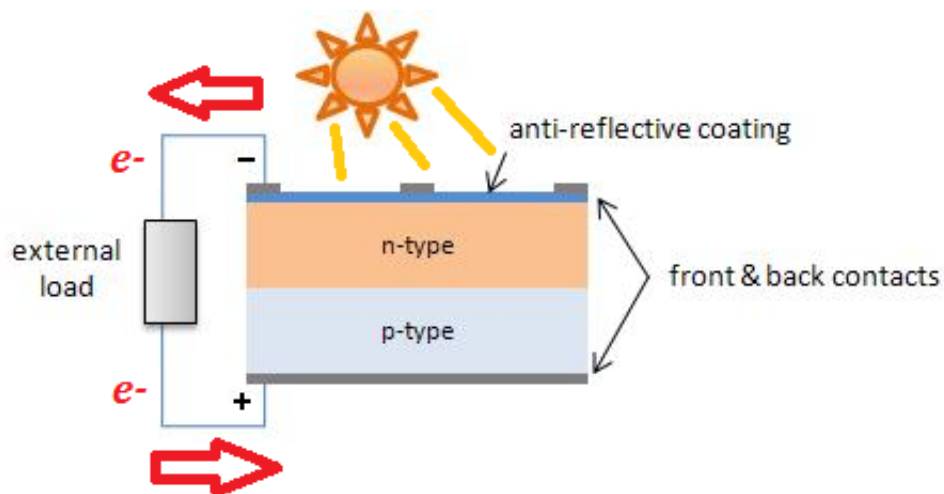


Figure 2.4: Solar cell working principles

As explained before there are many different types of solar cells due to their base material, their conversion spectrums and efficiencies. Every year National Renewable Energy Laboratory (NREL) of the USA publishes a chart [6] showing the past of the solar cell efficiencies and the most efficient cells that is produced today. These efficiency records are a good way of observing how solar cell technology evolved up to today from its first discovery and production in 1975. It is important to keep in mind that these efficiencies are for the cells produced in laboratory conditions and not for commercial use. However as they are technology demonstrators for today, they will be on the shelves for end-users in a couple of years, because the efficiencies keep increasing by the wide range of researches on this field. This chart for 2015 is given in Figure 2.5.

Best Research-Cell Efficiencies

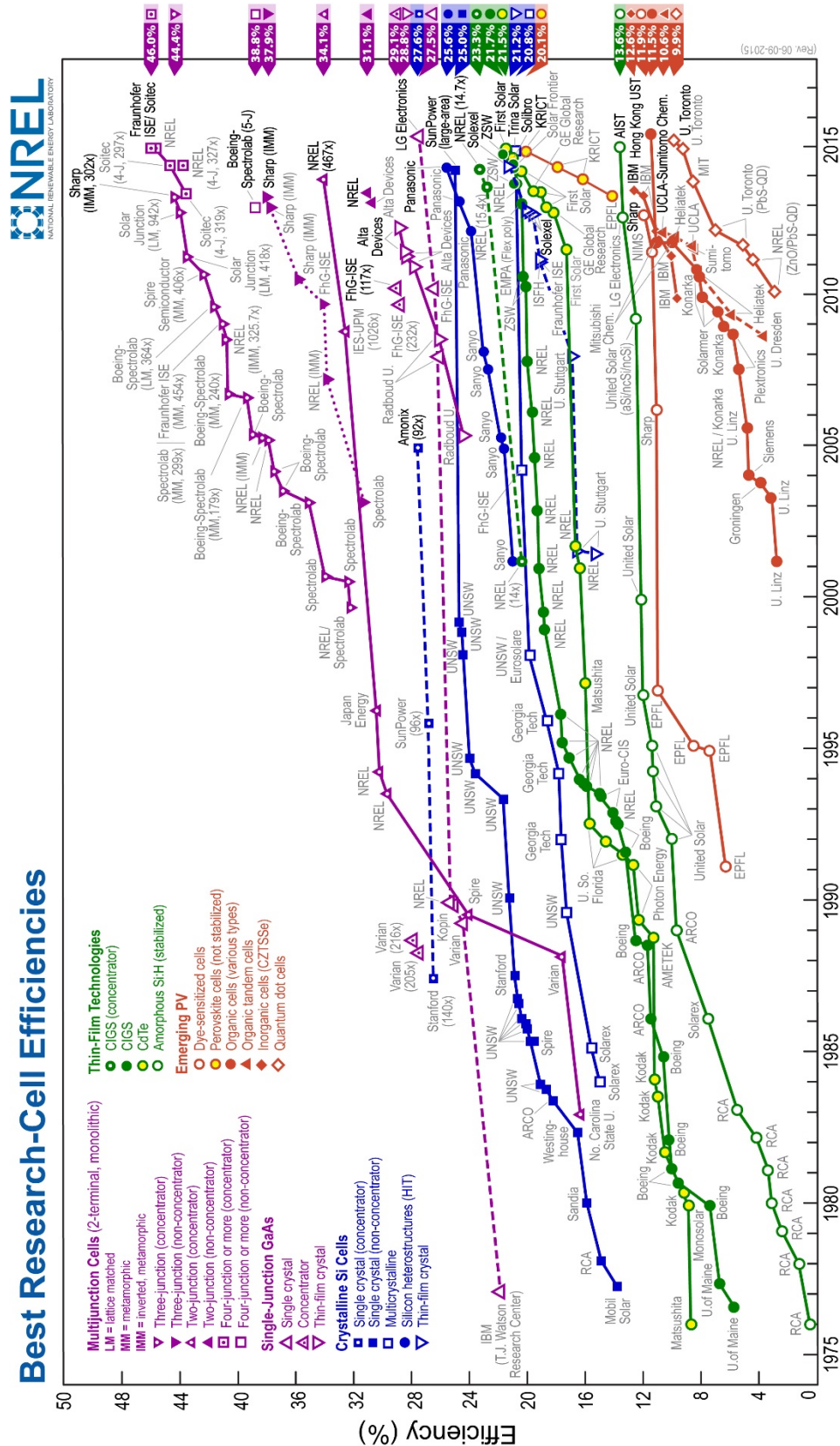


Figure 2.5: History of Cell Efficiencies [6]

For this thesis work, polycrystalline Silicon cells are planned to be used as their conversion efficiencies are 17-18% and they are easy to find in the market and to purchase as their cost is 0.78 \$/W. Looking at this chart for today, it can be easily seen that these cheap solar panels were the record holders for their class back in 1990. Therefore, with this fast advancement in photovoltaic (PV) solar cell technology, it is important to restate the possibility of seeing the cutting-edge efficiencies of today on the shelves in a couple of years.

2.3 CONCEPTUAL DESIGN

2.3.1 INITIAL SIZING

As it can be observed from the basic concepts about the flying wings, this type of aircraft has its own method of design. As only wings are designed the steps are fluent and iterative.

First of all the design requirements and inputs are determined as the starting point. The required inputs are as follows:

- Total mass (m)
- Wing Span (b)
- Root Chord Length (l_r)
- Tip Chord Length (l_t)
- Sweep Angle at $c/4$ ($\phi_{0.25}$)
- Design Lift Coefficient (c_L)
- Root Section Moment Coefficient ($c_{m,r}$)
- Root Section zero lift angle ($\alpha_{0,r}$)
- Tip Section Moment Coefficient ($c_{m,t}$)
- Tip Section zero lift angle ($\alpha_{0,t}$)
- Desired Stability Coefficient (σ)

It is also important to choose a suitable cruise altitude for this UAV, as it is solar powered it should fly as high as possible to avoid the clouds. Looking at Earth's atmosphere, 95% of horizontal clouds cannot pass 2000 m MSL limit. In order to fill in these inputs, a search for suitable reflexed airfoil is initiated. As this UAV will be solar powered, the solar cells placed on the wings should have the same orientation for ease of solar energy collection calculations and panel orientations. Therefore the root and tip airfoils are decided to be chosen differently to get the advantage of aerodynamic twist instead of geometric twist. The calculations for twist will be also done to make the geometric twist as close to zero as possible. As a result, the root and tip section airfoils are chosen first with respect to their moment coefficients and zero lift angles, through a search from various reflexed airfoils. After this search two suitable airfoils are found:

- E 186 - Eppler E186 Low Reynolds Number Airfoil This airfoil, shown in Figure 2.6, is found suitable as it is a flight-proven successful flying wing airfoil with comparatively high lift coefficient, and low moment coefficient. Its thickness to chord ratio of 10.27% is also useful as it provides enough thickness to house the equipment, avionics and batteries. Therefore it is chosen as the root airfoil.

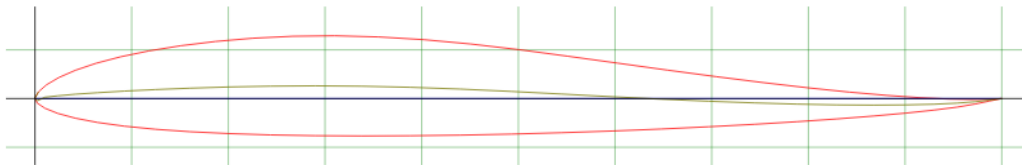


Figure 2.6: E 186 airfoil [11]

- MH 61 - Martin Hepperle MH 61 for Flying Wings This airfoil, shown in Figure 2.7, is found suitable as it matches E 186 with its similar characteristics. It is therefore chosen as the tip airfoil.

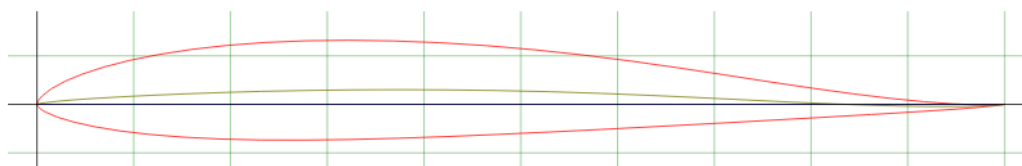


Figure 2.7: MH 61 airfoil [12]

In order to get the necessary data from these airfoils, the polars must be drawn for a given Reynold's number (Re). Re for the flight conditions of this solar powered UAV is calculated to be 2×10^5 for desired cruise speed of 12.5 m/s and cruise altitude of 2000 m MSL. The polars for these two airfoils were drawn for $Re = 2 \times 10^5$, and are shown in Figure 2.8 and Figure 2.9.

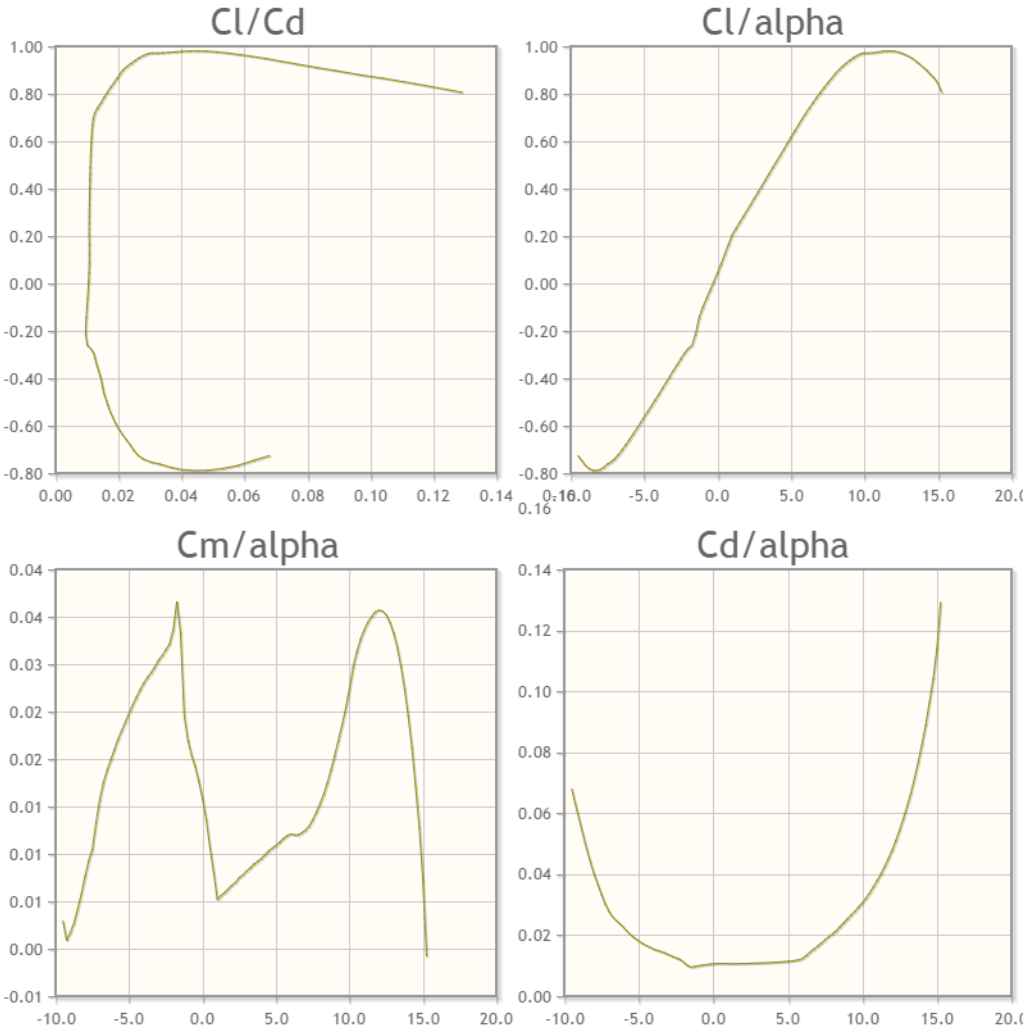


Figure 2.8: Polar curves of E 186 [11]

From these figures, the required data for both root and tip airfoils are gathered and shown in Table 2.2.

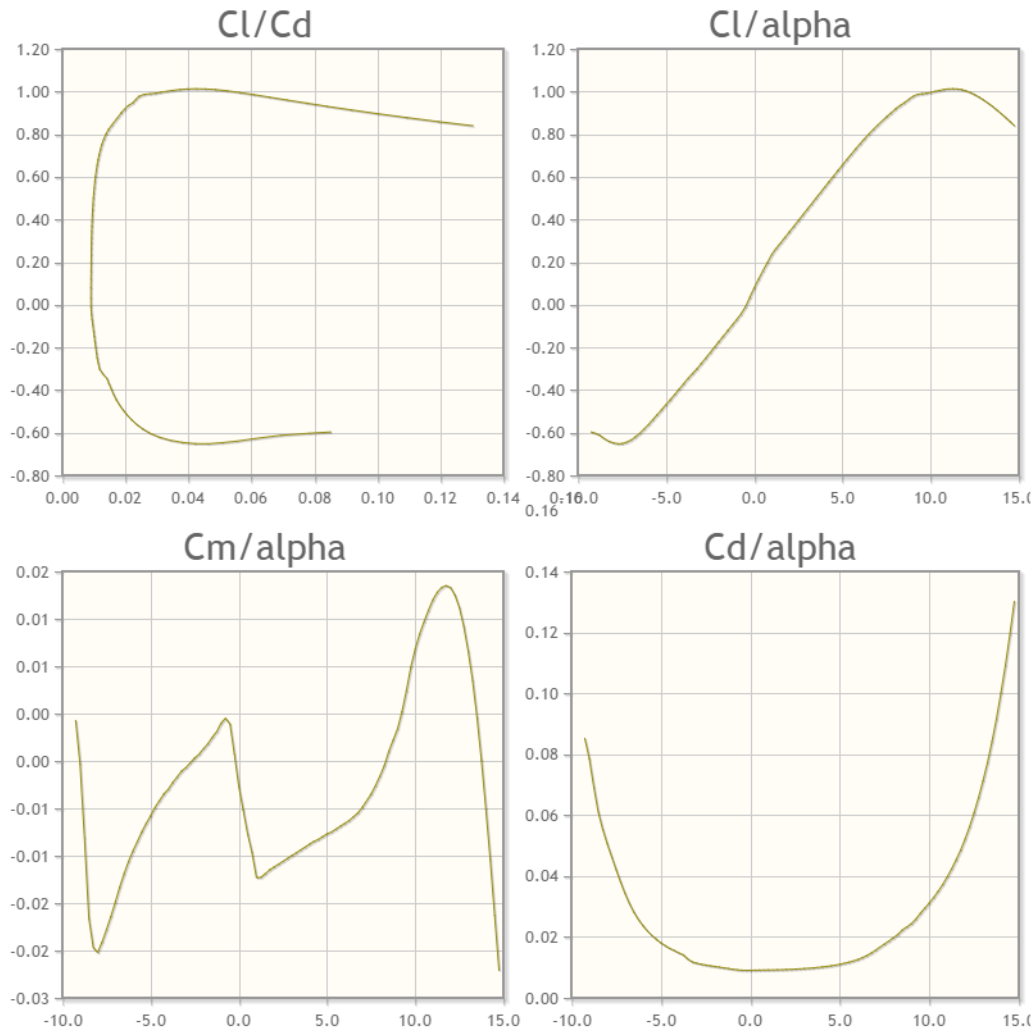


Figure 2.9: Polar curves of MH 61 [12]

Table 2.2: Moment coefficient and zero lift angle data of E 186 and MH 61 airfoils

E186	Root Section Moment Coefficient ($c_{m,r}$)	0.028
	Root Section zero lift angle ($\alpha_{0,r}$)	-0.75
MH 61	Tip Section Moment Coefficient ($c_{m,t}$)	0.015
	Tip Section zero lift angle ($\alpha_{0,t}$)	-0.31

After gathering these data about the airfoils and fixing them, rest of the required inputs are calculated, considering the following:

- Large wing area for high solar energy collection
- Long root chord length for fuselage formation

- High aspect ratio for low cruise speed and low drag

Through different iterations for the rest of the inputs, the suitable table of required inputs are formed and given in Table 2.3.

Table 2.3: Required inputs found after iterations and calculations

Wing Span (b) [m]	3.500
Root Chord Length (l_r) [m]	0.507
Tip Chord Length (l_t) [m]	0.135
Sweep Angle at c/4 ($\phi_{0.25}$) [degree]	21.7
Design Lift Coefficient (c_L)	0.500
Root Section Moment Coefficient ($c_{m,r}$)	0.028
Root Section zero lift angle ($\alpha_{0,r}$)	-0.75
Tip Section Moment Coefficient ($c_{m,t}$)	0.015
Tip Section zero lift angle ($\alpha_{0,t}$)	-0.31
Desired Stability Coefficient (σ)	0.05

By the help of fixing the initial sizing, it is now possible to find the geometric twist for longitudinal stability of this aircraft. In order to find geometric twist (β_{geo}), three steps of formulation from [3] should be followed:

1. Required twist (β_{req})

In order to find this value; AR, $\phi_{0.25}$, desired c_L and σ , standard c_L^* and σ^* should be known. AR is calculated and found as 10.9. Other values are directly taken from Table 2.3 and standard c_L^* is chosen as 1.00 and standard σ^* as 0.10, for general flying wings.

Using the graph to find standard β_{req}^* and formula shown in Figure 2.10 below;

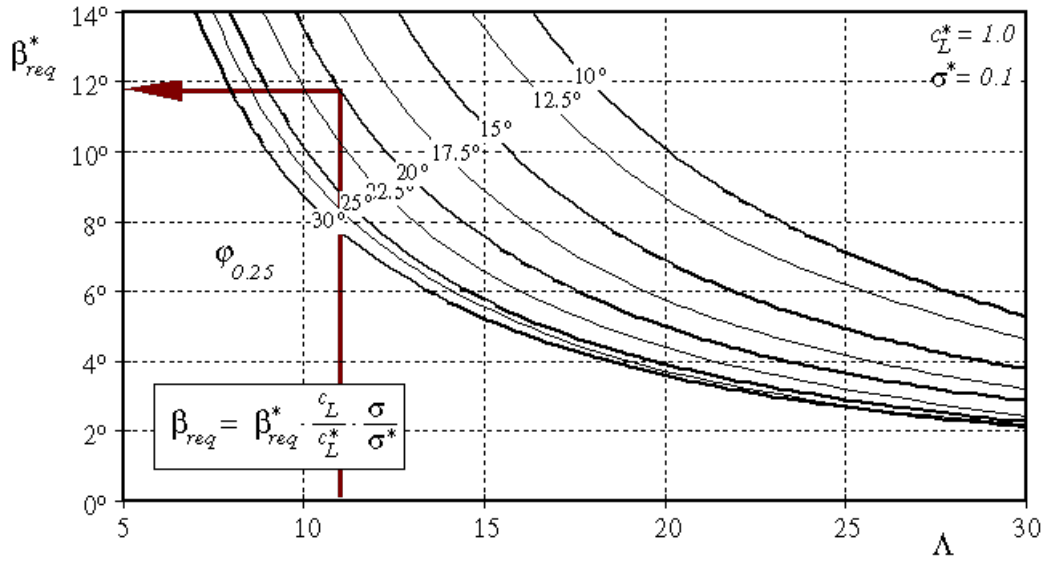


Figure 2.10: Graph of β_{req}^* vs AR for different $\phi_{0.25}$ and the equation to calculate β_{req}^* [3]

Therefore β_{req} is calculated as **2.81 degrees**.

2. Effect of zero lift angle ($\beta_{\alpha,0}$)

As different airfoils are used at roots and tips of the wings, the geometric twist will be reduced as much as their differences in zero lift angles. This value is calculated using Eqn. (2.5).

$$\beta_{\alpha,0} = \alpha_{0,tip} - \alpha_{0,root} \quad (2.5)$$

Therefore $\beta_{\alpha,0}$ is calculated as **0.44 edegrees**.

3. Effect of Moment Coefficients (β_{cm})

Using airfoils with positive moment coefficients contribute to lowering the geometric twist. This is also one of the reasons the reflexed airfoils are chosen for this solar powered UAV.

Taking c_m as the average of the moment coefficients of root and tip airfoils, and standard c_m^* as 0.05 for general flying wing designs, β_{cm} can be calculated by using the formula and graph shown in Figure 2.11 similar to finding the required twist.

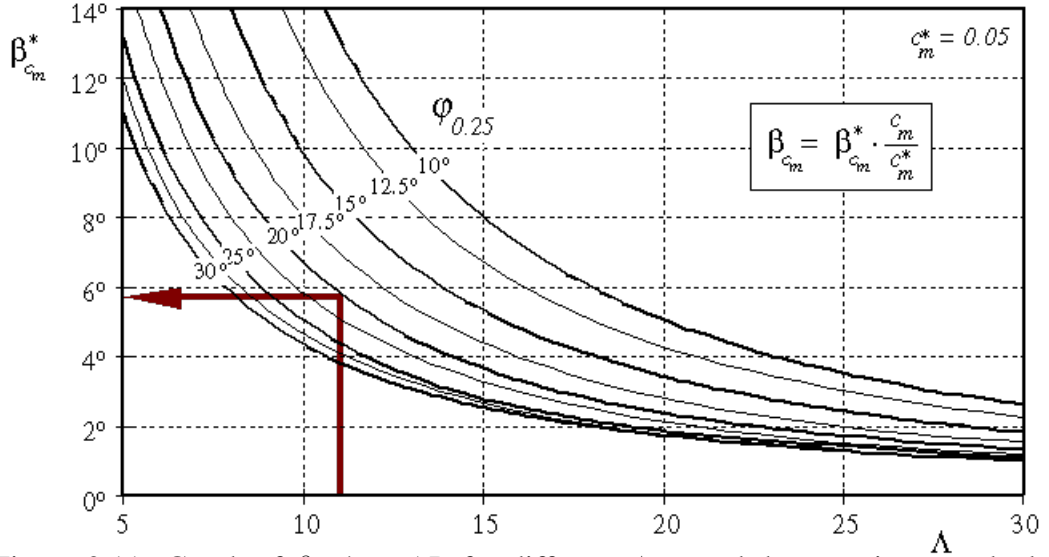


Figure 2.11: Graph of β_{cm}^* vs AR for different $\phi_{0.25}$ and the equation to calculate β_{cm}^* [3]

Therefore β_{cm} is calculated as **2.47 degrees**.

As a result, when all these steps are combined in Eqn. (2.6).

$$\beta_{geo} = \beta_{req} - \beta_{\alpha,0} - \beta_{cm} \quad (2.6)$$

β_{geo} is found as -0.10 degrees which is very close to zero so that it can be neglected. This shows that by using a good set of airfoils at the roots and tips, and combining them with suitable AR and $\phi_{0.25}$, the geometric twist requirement can be eliminated. It is possible to build the wing of the solar powered UAV without any difference in the spanwise orientation, which is extremely useful for panel placement and solar energy collection calculations.

After eliminating the geometric twist, general sizing of the aircraft is complete and the data gathered from conceptual design phase can be used for performance analysis and lastly 3D model of the prototype aircraft can be drawn for detail design and manufacturing phases.

2.4 PERFORMANCE ANALYSIS

2.4.1 WING LOADING

This UAV is a mini class UAV and the propulsion will be by electric motor, therefore no weight estimations for different phases of its flight envelope are made in the previous part. This gives the advantage of the weight of aircraft to be the same throughout its entire flight.

Considering the total estimated weight of the aircraft to be 4 kg, the wing loading can be simply calculated as W/S equal to 3.56 kg/m^2 , which is almost equal to that of glider class aircraft.

Using this value in Eqn. (2.7) [2] to find V_{stall} , where $c_{L_{max}}$ value is 2.1;

$$V_{stall} = \sqrt{\frac{W/Sg}{0.5\rho_{\infty}c_{L_{max}}}} \quad (2.7)$$

V_{stall} is calculated as 5.2 m/s which is low and therefore suitable for belly landing. This makes the aircraft even simpler, without the need of any other recovery system like parachute or airbag.

2.4.2 POWER AVAILABLE AND POWER REQUIRED CURVES

Power system and management of a solar powered UAV is very critical for its endurance. As the UAV is being designed to achieve high performance aerodynamically, the power system should also be designed as efficiently as possible. Power system on board of the solar powered UAV can be described as schematics in Figure 2.12. As shown in this figure, the solar cells supply voltage and current to MPPT. Then MPPT converts this voltage and current so that it efficiently matches recharging voltage of the batteries and current draw by avionics on board. Therefore, power available will be calculated according to the solar power acquired from solar cells, efficiency of MPPT, ESC and propulsion unit (motor and propeller). As the rest of the avionics will be supplied by the BEC voltage of the ESC, power available found will cover all the demand.

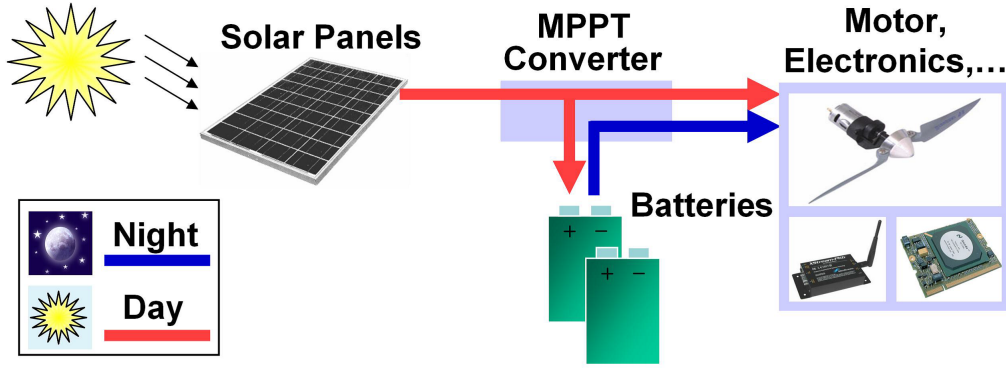


Figure 2.12: Power system of solar powered UAV [5]

For optimum power available calculations, incoming solar irradiation estimation should be done for the specific dates of flight. The profile will have three different panel alignments and as the wings are tapered, leading edge panels (LEP) can cover 0.18 m^2 at an angle of 18.5 degrees with horizontal; midchord panels (MCP) can cover 0.34 m^2 parallel to horizontal and trailing edge panels (TEP) can cover 0.52 m^2 at almost parallel to horizontal. As the UAV is planned to fly within one day time, for calculations the hourly integrated solar irradiation formula (Eqn 2.8) will be used;

$$I_0 = \frac{12 \times 3600}{\pi} G_{sc} \left[1 + 0.033 \cos \frac{360n}{365} \right] \times \left[\cos \phi \cos \delta (\sin \omega_2 - \sin \omega_1) + \frac{\pi(\omega_2 - \omega_1)}{180} \sin \phi \sin \delta \right] \quad (2.8)$$

Following describes the variables given in Eqn. (2.8) for a day in June and for an average time:

G_{sc} : Solar constant = 1367 W/m^2

n : day number = June 11_{th} = 162

δ : Declination = 23,1 (for June 11_{th}) [1]

ϕ : Latitude of the position of the UAV [1]

ω : Time of the day converted to degrees (12:00 being 0 and for each hour 15 degrees is added or subtracted) [1]

The geometric factor R_b (2.9 [1]) will also be used as there are three different align-

ments of solar panels:

$$R_b = \frac{G_{bT}}{G_b} = \frac{G_{bn} \cos \theta}{G_{bn} \cos \theta_z} = \frac{\cos \theta}{\cos \theta_z} \quad (2.9)$$

In which;

$$\cos \theta = \sin \delta \sin (\phi - \beta) + \cos \delta \cos (\phi - \beta) \cos \omega \quad (2.10)$$

$$\cos \theta_z = \frac{G_{bT}}{G_b} = \frac{G_{bn} \cos \theta}{G_{bn} \cos \theta_z} = \frac{\cos \theta}{\cos \theta_z} \quad (2.11)$$

In Eqn (2.10) and Eqn (2.11); β stands for the inclination angles of the panels which were mentioned before. In the following, detailed calculations for each panel in Ankara for June 11th will be given only as an example, as the days of flight are unknown for now.

Latitude of Ankara is 40 degrees North.

The times of the day the UAV is in the air;

For 10:00; $\omega_1 = 15 \times (10 - 12) = -30$

For 11:30; $\omega_2 = 15 \times (11.5 - 12) = -7.5$

For the LEP;

Area of LEP = $0.18m^2$

$\beta = 18.5$ degrees

From these values and Eqn. (from 2.8 to 2.11);

$\cos \theta = 0.97$

$\cos \theta_z = 0.93$

$R_b = 1.04$

$I_0 = 6.55 \times 10^6 J$

$I_{estimated} = I_0 \times R_b = (6.55 \times 10^6) \times (1.04) = 6.81 \times 10^6 J/m^2$

Energy acquired : $I_{estimated} \times Area = (6.81 \times 10^6) \times (0.18) = 1.23 \times 10^6 J$

For the MCP;

Area of MCP = $0.34m^2$

$\beta = 0$ degrees (parallel to horizontal)

From these values and Eqn. (from 2.8 to 2.11);

$$\cos \theta = 0.93$$

$$\cos \theta_z = 0.93$$

$$R_b = 1$$

$$I_0 = 6.55 \times 10^6 J$$

$$I_{estimated} = I_0 \times R_b = (6.55 \times 10^6) \times (1) = 6.55 \times 10^6 J/m^2$$

$$\text{Energy acquired : } I_{estimated} \times Area = (6.55 \times 10^6) \times (0.34) = 2.23 \times 10^6 J$$

For the TEP;

$$\text{Area of TEP} = 0.52 m^2$$

$$\beta = 0 \text{ degrees (almost parallel to horizontal)}$$

From these values and Eqn. (from 2.8 to 2.11);

$$\cos \theta = 0.83$$

$$\cos \theta_z = 0.93$$

$$R_b = 1$$

$$I_0 = 6.55 \times 10^6 J$$

$$I_{estimated} = I_0 \times R_b = (6.55 \times 10^6) \times (1) = 6.55 \times 10^6 J/m^2$$

$$\text{Energy acquired : } I_{estimated} \times Area = (6.55 \times 10^6) \times (0.52) = 3.41 \times 10^6 J$$

As a result total energy acquired at that day will be $6.87 \times 10^6 J$ for 1.5 hours of flight.

When converted to power it means that incoming power is $1272 W/m^2$. This can be used instead of average incoming solar power, which is $900 W/m^2$, when the days of flight are certain for better solar power collection estimation. This is given only as an example to the detailed calculations that will be done for analysis in final flight testing. For the general performance analysis the power acquired will be calculated on average values, because the days of flight are unknown as mentioned before.

Therefore to find available power, the power acquired from the solar cells must be calculated. The solar cells chosen for this thesis work are polycrystalline silicon solar cells with conversion efficiencies of 17-18%. The properties of the chosen solar cell are given in Table 2.4.

Table 2.4: Chosen solar cell properties

Size (mm) (length x width x thickness)	156 x 52 x 0.1
I_{MPPT} (Current at Maximum Power) (A)	2.2
V_{MPPT} (Voltage at Maximum Power) (V)	0.6
P_{MPPT} (Power at Maximum Power) (W)	1.32
η_{sol} (Conversion Efficiency)	0.176

Considering the total upper surface area of wings and fuselage is $1.25m^2$. If the UAV were to be covered entirely with these panels, the power collected for an average day can be calculated using Eqn. (2.12)

$$P_{sol} = S_{total}\eta_{sol}(900\frac{W}{m^2}) \quad (2.12)$$

From this equation, P_{sol} is found as 198 W. As this is the ideal case, P_{sol} is calculated again using Eqn. (2.12) but using the maximum possible covered area by the solar cells, $S_{covered}$. From the placement of the cells on the wings it is found that 128 cells are needed to cover as much area as possible. The total area of 105 cells is $0.85 m^2$ which actually gives $S_{covered}$. As a result P_{sol} is recalculated and found to be 138.6 W.

Finally, using this value in Eqn (2.13);

$$P_{av} = P_{sol}\eta_{MPPT}\eta_{ESC}\eta_{prop} \quad (2.13)$$

Along with respective efficiencies of 0.98, 0.98 and 0.85; P_{av} is calculated as 113.1 W. This value is calculated for an average day and detailed calculations will be made at final flight testing specifically for the days of flight, as presented in the paper [1] as a part of this thesis work.

Using the power requirements from drag calculations the power required and power available curves are drawn and shown in Figure 2.13. As seen in this figure, lowest required power is 30 W and for the desired cruise speed of 12.5 m/s the required power is 46 W which is 40% of readily available power supplied by solar cells. This shows that there will be enough power to sustain cruise flight and to charge the batteries

which may be depleted during climb. This difference in required and available power values is a very important advantage for the solar UAV designed to be successful.

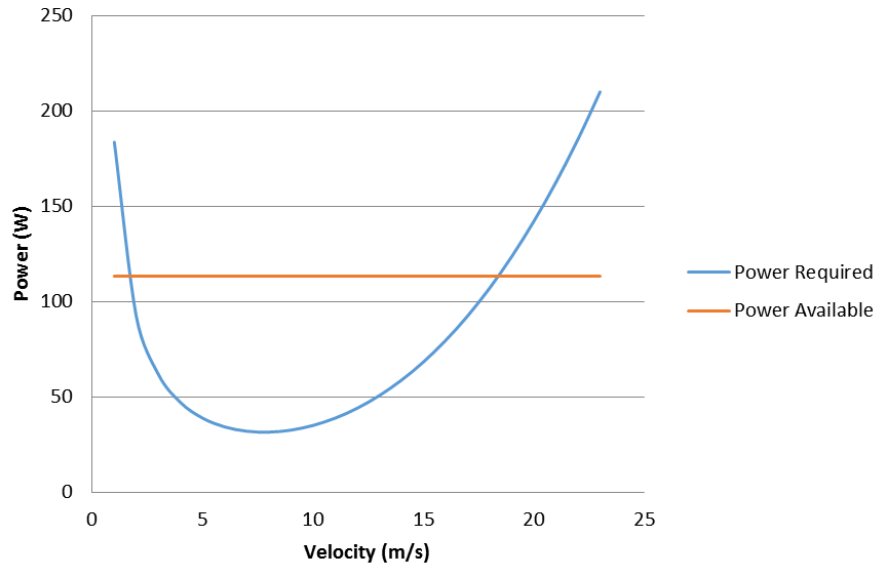


Figure 2.13: Power vs velocity curves

2.4.3 RATE OF CLIMB AND TIME OF CLIMB

The rate of climb is calculated from the excess power and difference in the lift force and weight at maximum power use by physics approach as shown in Eqn. (2.14).

$$V_{vertical} = \frac{P_{excess}}{L - W_{@max}} \quad (2.14)$$

The resulting rate of climb ($V_{vertical}$) is found as 1.25 m/s. This result is a good estimate as the calculation is done on using the incoming solar power only, without getting excessive power from the batteries. At this rate, the solar powered UAV is estimated to climb to 2000 m MSL in 26.5 minutes. This can be shortened with the use of excessive power from batteries.

2.5 DESIGN OUTPUTS AND 3-D MODEL

Looking at the performance analysis, the conceptual and preliminary design phases can be concluded and the UAV can be modeled in CATIA for detail design and man-

ufacturing. In addition to the model, in order to increase effective λ , transparent winglets are decided to be used.

The summary of design parameters is shown in Table 2.5.

Table 2.5: Design parameters

Wing Span (b) [m]	3.500
Root Chord Length (l_r) [m]	0.507
Tip Chord Length (l_t) [m]	0.135
Sweep Angle at c/4 ($\phi_{0.25}$) [degree]	21.7
Wing Area (S) [m^2]	1.12
Aspect Ratio (λ)	10.89
End Plate Height (EP) [m]	0.25
Effective AR (λ_{eff})	12.37
Location of Neutral Point (x_N) [m]	0.408
Location of c.g (x_{CG}) [m]	0.39
Stability Margin (%)	5.11

According to these parameters, the 3-D model of the prototype solar powered UAV is drawn in CATIA. The fully assembled model and ISO views are shown in Figure 2.14 and Figure 2.15 respectively.



Figure 2.14: Fully assembled UAV

From the 3-D model, weight estimations are made for the first prototype of the UAV. The estimations are shown in Table 2.6.

Table 2.6: Estimated Weight Distribution

Part	Estimated Weight (gr)
UAV Structure	1800
Avionics (Motor, Battery etc.)	1000
Solar Cells and Charging Circuit	600
Payload and Communications	600
TOTAL	4000

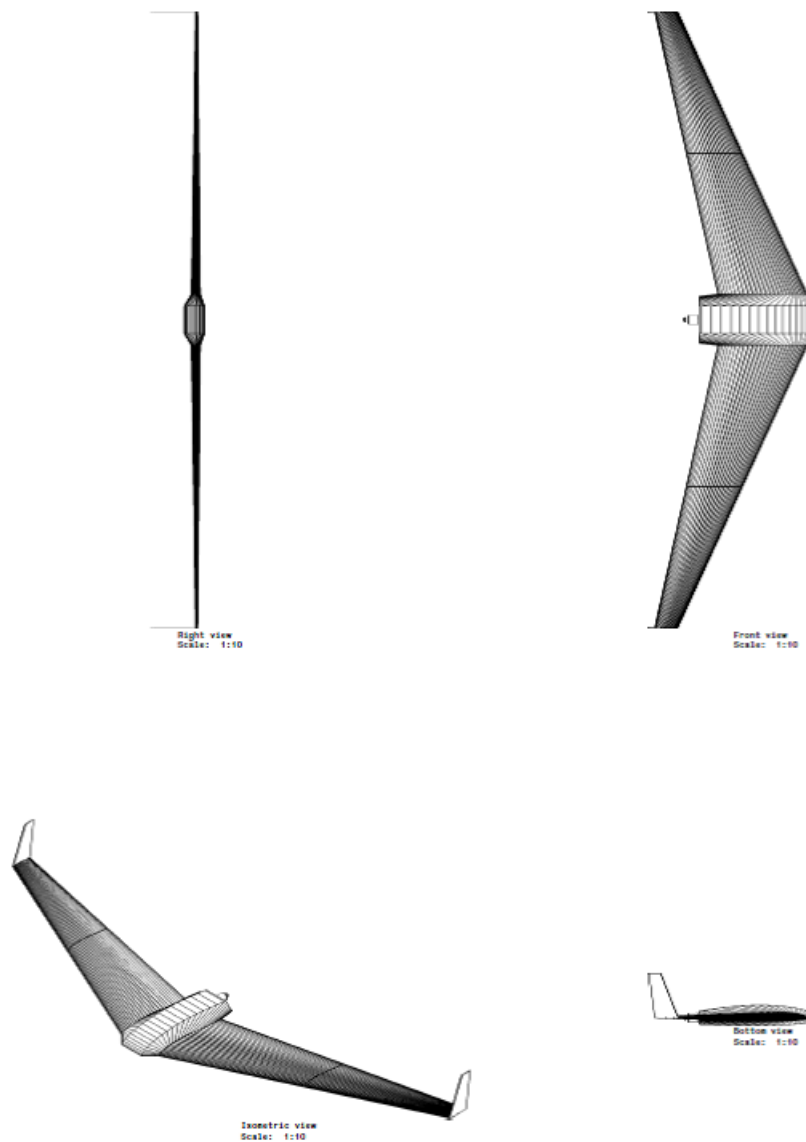


Figure 2.15: Front, top, ISO and side views of the solar powered UAV design

2.6 MATERIAL SELECTION

The UAV will be produced from EPS or EPP foam, for ease of production and for creating a solid fill under solar panels for support. EPP foam is a lightweight, strong, semi-flexible material with reforming structure. On the other hand EPS foam is also lightweight and strong but is less flexible with respect to EPP. The UAV is planned to be produced by hot wire cutting technique therefore foam blocks or panels will be required. It is hard to find EPP foam blocks commercially, especially in Turkey; as parts from EPP are mainly produced by injection molds. However EPS foam blocks are easy to find, therefore EPS will be used for production.

The EPS foam come in different densities from 16 to $30\text{kg}/\text{m}^3$. This type of foam is less flexible and more brittle than EPP therefore for safety in structural stiffness for the first prototype production high density EPS is chosen to be used. The EPS foam chosen to be used for this production has a density of $26\text{kg}/\text{m}^3$.

For supporting structural elements, such as spars and end ribs, carbon-balsa composite rectangular rods, carbon fiber cylindrical rods and 1.5 mm carbon fiber plates will be used. These materials and shapes are chosen so that the structure is stiff enough in order not to break solar cells during flight or landing.

Winglets will be produced from 3 mm Plexiglas plates, as they need to be strong and transparent in order not to cast shadow over solar cells.

All these parts will be stuck together by UHUPOR styro-foam glue, as many other types of adhesives can melt through foam. This adhesive has low density and short curing time, therefore is suitable for the production of this UAV.

CHAPTER 3

MANUFACTURING

3.1 PRODUCTION OF MAIN PARTS

As the main parts are built from EPS foam, the manufacturing plan is chosen so that it would provide sufficiently stiff and supportive structure for solar cells on one hand and on the other, most lightweight structure that is both time and cost efficient in terms of production. The manufacturing processes to match these criteria for each main part are described in the following parts. Hot wire cutting technique is the most frequent, reliable and simple method in shaping and cutting the foam; thus, this technique is chosen.

The aircraft consists of seven main parts, as shown in Figure 3.1 :

- Fuselage
- Left and Right Wing Piece 1
- Left and Right Wing Piece 2
- Left and Right Winglets

Each part is cut at different lengths for easy assembly-disassembly and transportation. Fuselage has a width of 29.4 cm and each wing part has a length of 80 cm spanwise, “Wing Piece 2” parts connect with 3 mm thick plexiglas winglets, adding up to the total wing span of 350 cm when assembled.

The production began by producing wings as two pieces each (Piece 1 and Piece 2) by hot wire CNC foam cutter as shown in Figure 3.2.

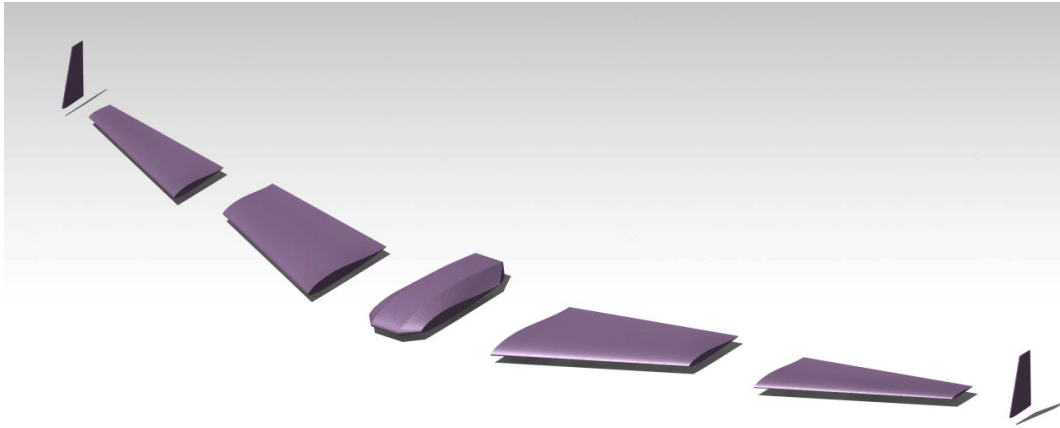


Figure 3.1: Main parts of the UAV

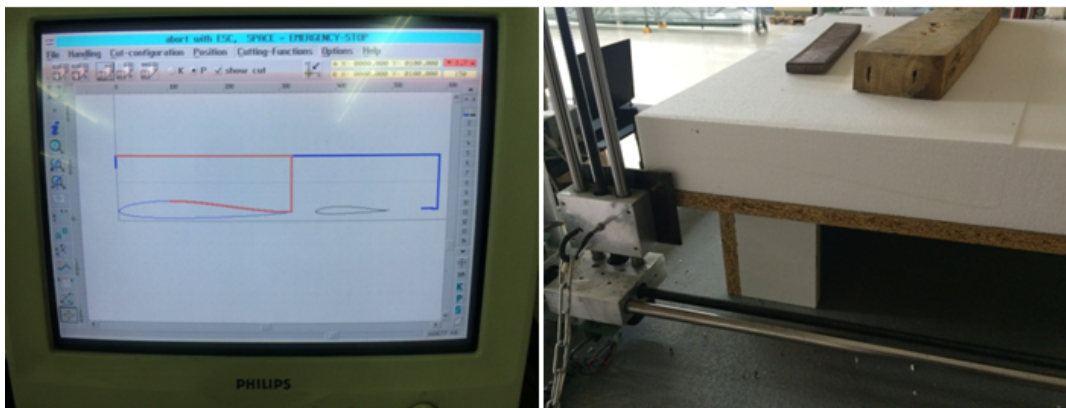


Figure 3.2: Production of Wing Piece 1 and 2 in hot wire CNC foam cutter

After the wings are cut by hot wire, the surfaces and dimensions are checked for any possible errors. As mentioned before, profile geometry, geometric alignment and dimensions are extremely important in flying wing design; any possible error in production can lead to irrecoverable instability during flight. In addition, as a side benefit of hot wire foam cutting, when the part is produced, rest of the foam is shaped as two female molds for both upper and lower surfaces of the part. These “molds” will be used during production phase as base plate, so their surface qualities are also important. Checking both after each part production, shown in Figure 3.3, the surface quality of all parts and molds are found to be good.



Figure 3.3: Surface quality check for produced part

Fuselage is also cut by hot wire, but in two steps as it has a more complex shape than wings and is needed to blend to the wings. Firstly, the middle profile for the fuselage is cut. Then the cut part is turned 90 degrees and the front cross-section is given as the cutting path to the hot wire router, creating the necessary side slopes for blending to the wings. The middle profile and final fuselage shape are shown in Figure 3.4.

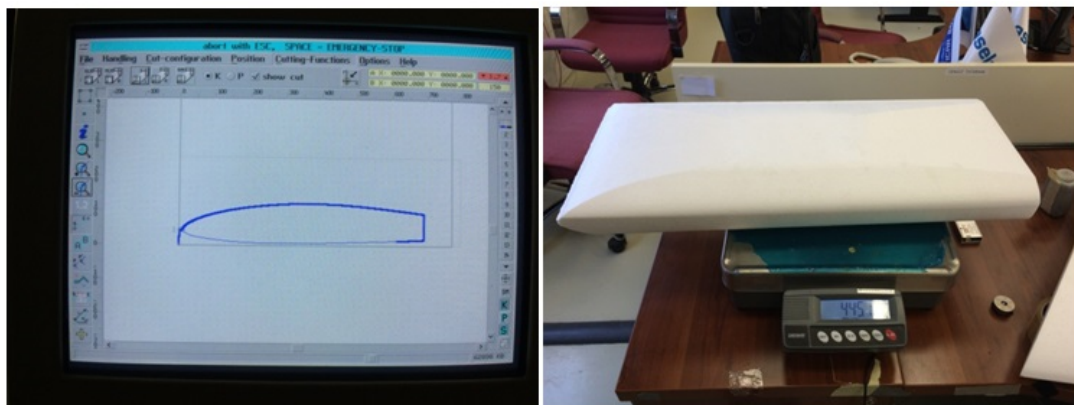


Figure 3.4: Production of fuselage and the produced part

This part is also checked for surface quality, dimensions and errors. After all parts are checked, they are all weighed and weights are recorded. Weights of each part can be seen in Figure 20.

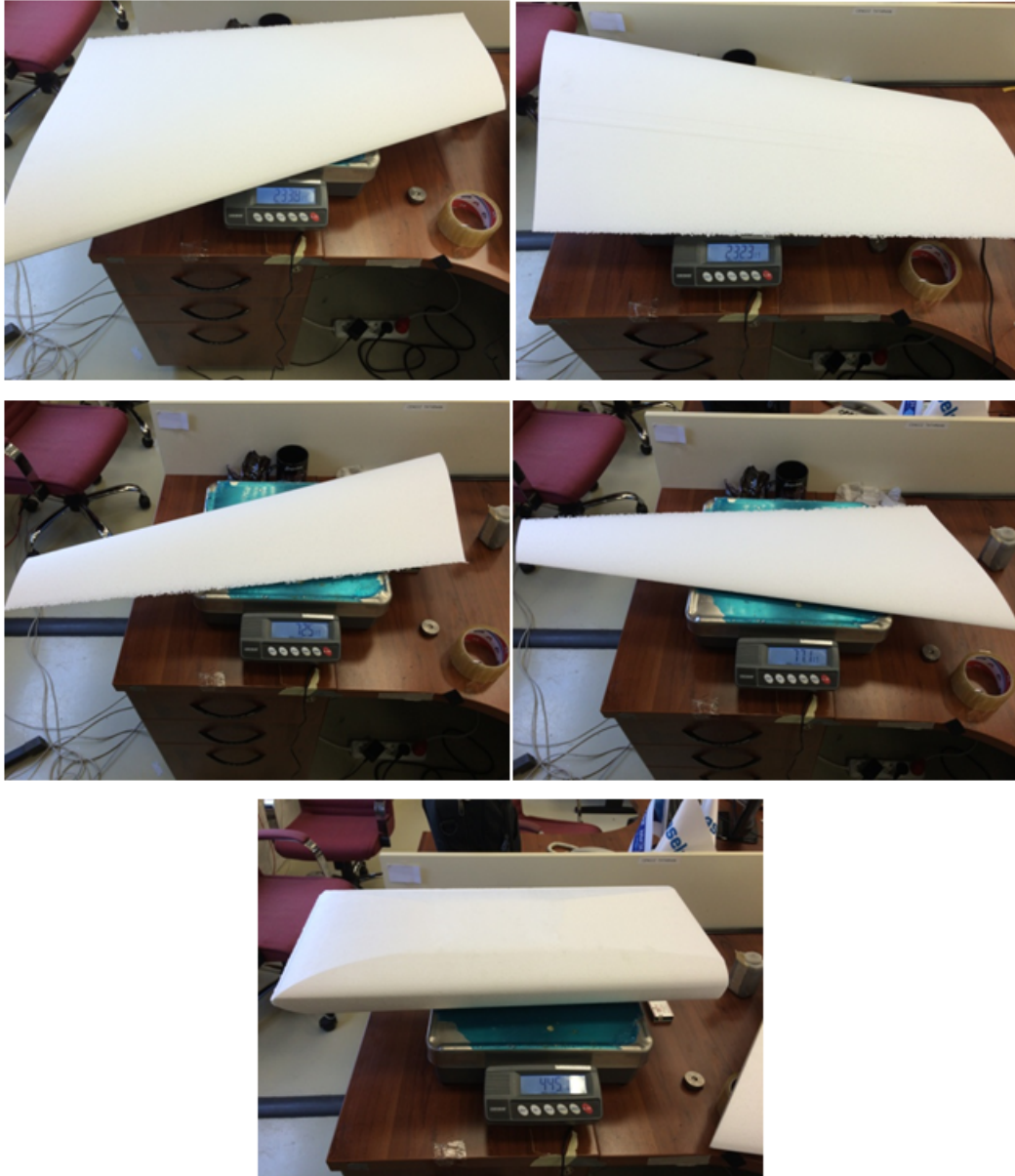


Figure 3.5: Weights of foam parts

The weights add up to 1060 grams. Some parts will be cut and hollowed so that the total weight will be less when the parts are ready for internal structure assembly. According to the estimation and considering this possible loss in weight, around 800 grams will be left for internal structure elements, control surfaces and craftsmanship. Winglets are also an additional weight to be considered.

3.2 INTEGRATION OF STRUCTURAL ELEMENTS

3.2.1 PRODUCTION OF STRUCTURAL ELEMENTS

There are three types of structural elements that will be integrated to this UAV structure. These elements are chosen to provide the required stiffness to the overall structure and easy assembly-disassembly. The elements are as follows:

- *Rectangular Carbon fiber - Balsa Wood Composite Spars*; for lightweight and overall stiffness to prevent dihedral formation during flight, three rectangular spars will be integrated inside the wings.
- *Cylindrical Carbon fiber Rods* ; for lightweight connection spars.
- *1.5 mm Carbon fiber Plate End Ribs* ; for stiff support in connection areas as well as support and interconnection to the main rectangular spars and connection spars.

Each of these elements is produced separately as they will be made of different materials.

Firstly, rectangular composite spars are produced. For that 4 mm balsa wood is covered with 2 layers of Carbon fiber and cured in room conditions. The produced composite spars are shown in Figure 3.6.

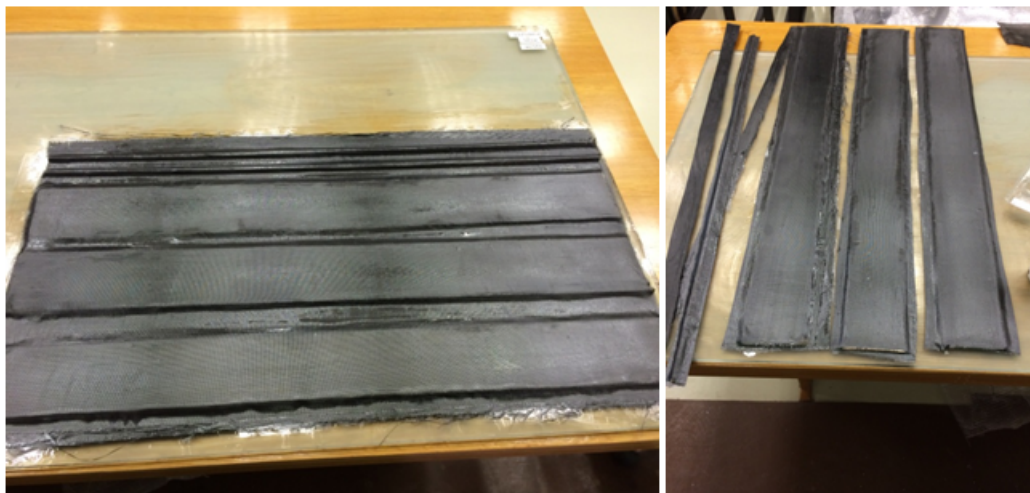


Figure 3.6: Production of Rectangular Composite Spars

Secondly, cylindrical carbon fiber rods are cut from manufactured rods with specific diameters; 8, 10, 16 and 18 mm. The lengths of the rods are determined from the 3D design in CATIA, as shown in Figure 3.7.

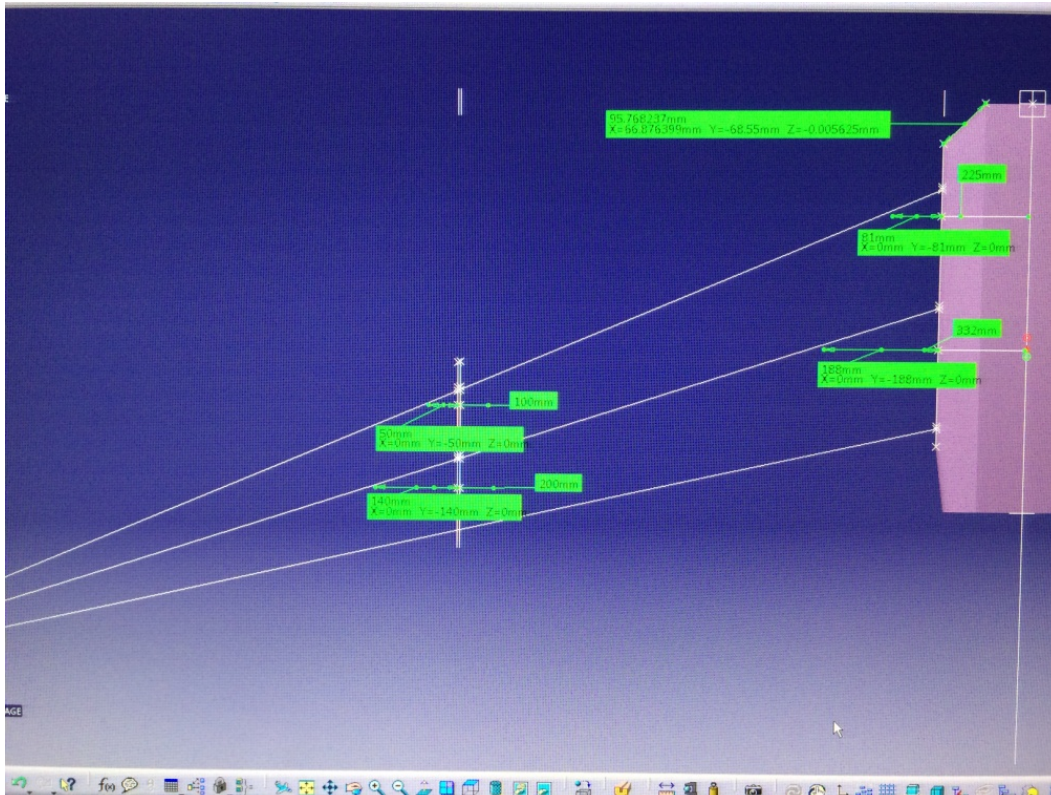


Figure 3.7: Lengths and positions of connection spars with respect to rectangular spars and end ribs

After the lengths of the rods for each diameter is determined, they are cut, trimmed and labeled for their positions. The rods can be seen in Figure 3.8.

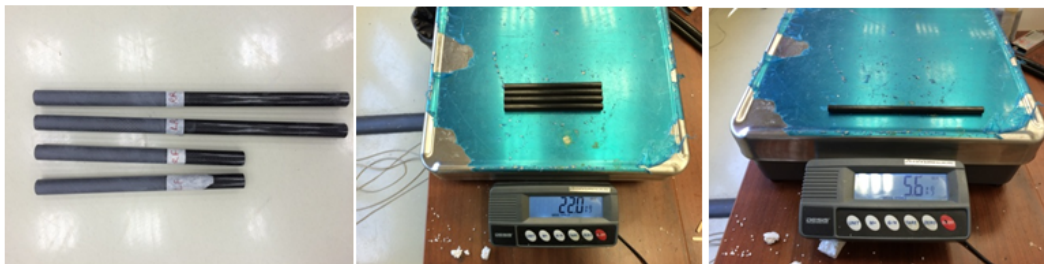


Figure 3.8: Production of Connection Rods

Lastly, end ribs are cut from 1.5 mm carbon fiber plate. In order to cut the end ribs, templates for the end ribs are created in CATIA, printed out and stuck on the plate.

These end ribs are then cut out by Dremel, and spar connection holes are drilled. The templates and the production of the end ribs are shown in Figures 3.9 and 3.10.

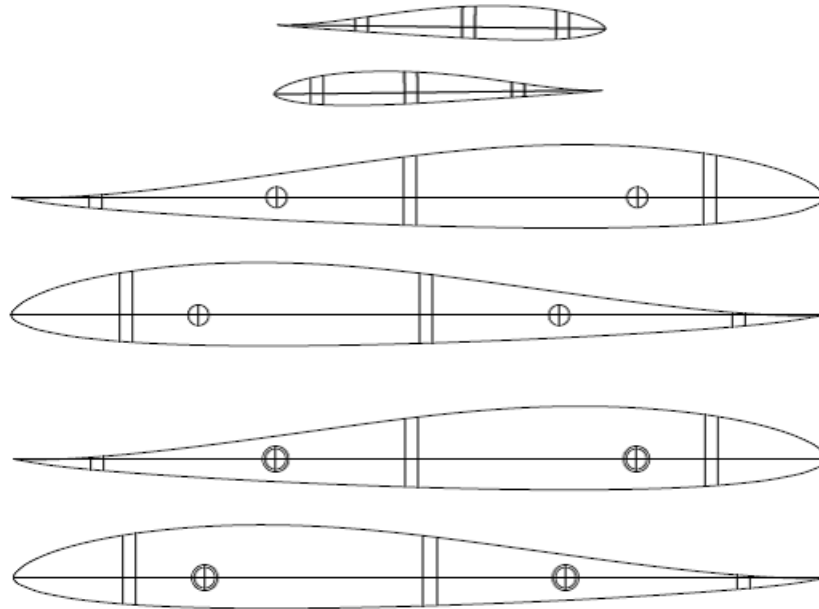


Figure 3.9: Templates for the end ribs with the positions of connection and main spars

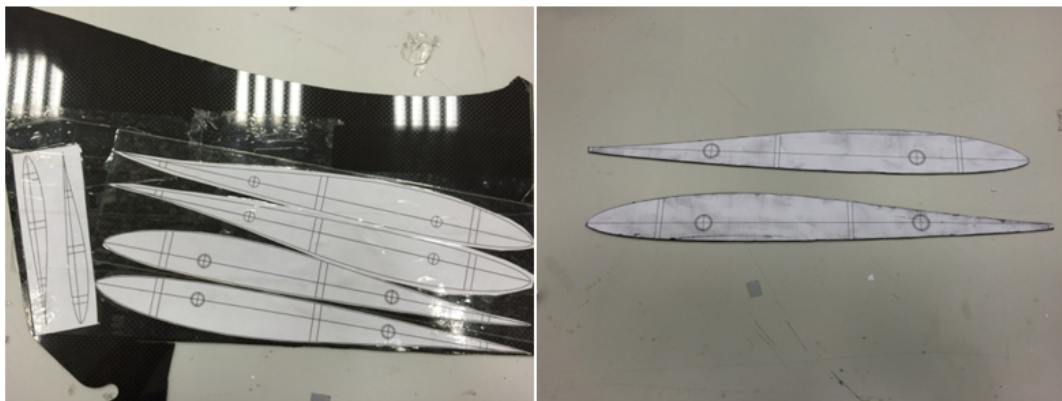


Figure 3.10: Production of 1.5 mm carbon fiber plate end ribs

After the production of structural elements, these elements are integrated into Left and Right Wing Piece 2, Left and Right Wing Piece 1 and Fuselage, from outside to inside to maintain structural continuity.

3.2.2 INTEGRATION TO WING PIECE 2

Firstly, end ribs are glued on the tip and root parts of Wing Piece 1. They are left for half an hour to be cured and hardened. After that, the location of the control surface and the rear rectangular spar is drawn as guide on the part. These steps are shown in Figure 3.11.

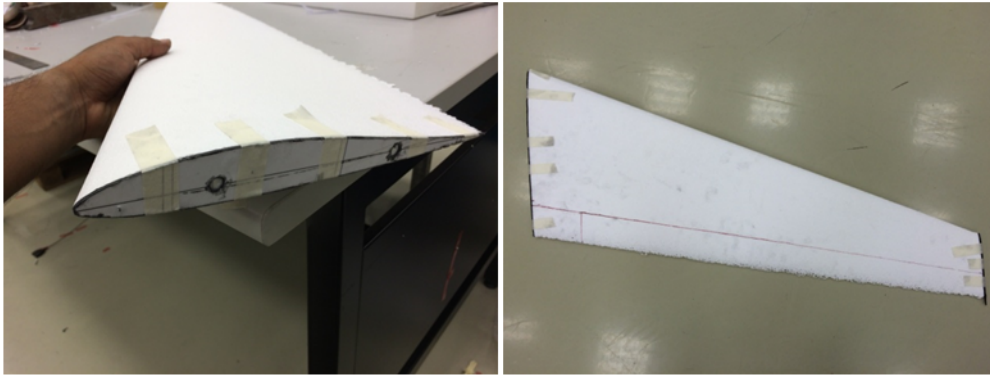


Figure 3.11: Gluing of the end ribs and drawing the control surface and rear spar location

Then, the foam on control surface location and rear spar location are removed by scalpel. Rear rectangular spar is glued to its position. Control surface is also cut aside using the removed foam as template and brought into its position to check if trimming is required. These steps are shown in Figure 3.12.



Figure 3.12: Gluing of rear spar and control surface production

After the rear spar is glued tight, the part is turned upside down, placed on the upper side mold and the locations for the middle and front spars are drawn. The foam in

these locations is removed by using Dremel and tunnels for middle and front spars are formed. The locations where rectangular spars will go out on the end ribs are also removed. Finally these two spars are glued into their respective locations, as shown in Figure 3.13.

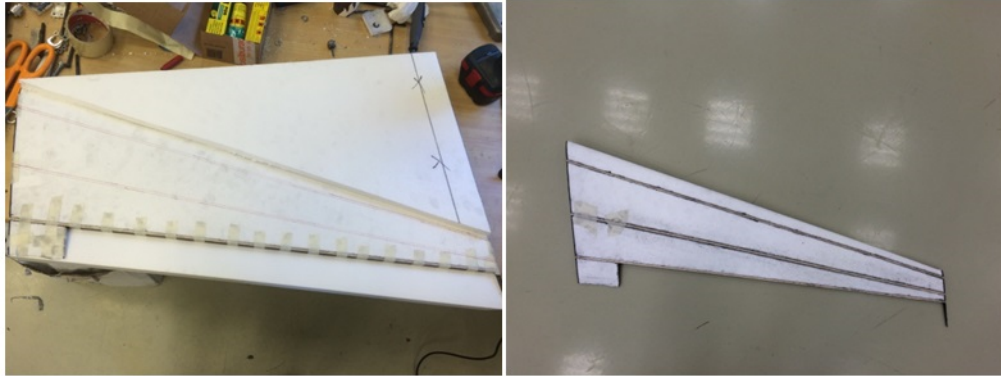


Figure 3.13: Drawing locations for rectangular spars and their integration into the part

After the glue is cured, the part is put on its upper surface mold again for connection spar integration. Open holes on the root end rib act as the guide for these connection spars. Using these holes and lengths drawn on the direction of insertion, 6 mm holes are drilled to the foam for certain lengths given before. 8 mm connection spars are then inserted into these holes by rolling and pushing in for tight fitting. To prevent the foam from being ripped apart, the inserted side of the connection spar is shaped as teeth by Dremel. When the tunnels are ready, they are slightly filled with glue and the spars are inserted into their places. These steps are shown in Figure 3.14.



Figure 3.14: Drawing guide lines, shaping one side of the spar as teeth and integration of spars

The part is left for a day to cure completely. It is checked for any excess parts and is trimmed by Dremel if there are any. These steps are then repeated for the other Wing Piece 2.

3.2.3 INTEGRATION TO WING PIECE 1

Production of Wing Piece 1 is similar to Wing Piece 2. Firstly, end ribs are glued on the tip and root part of Wing Piece 1. They are left for half an hour to be cured and hardened. After that, the part is put on its upper surface mold and locations of three rectangular spars are drawn as guide on the part. The continuity of these locations with Wing Piece 1 is checked. These steps are shown in Figure 3.15.

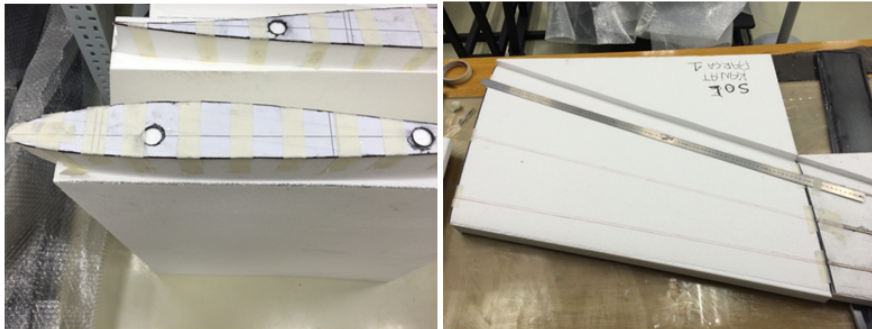


Figure 3.15: Gluing of the end ribs and drawing the spar locations

The foam in these locations is removed by using Dremel and tunnels for the three spars are formed. The locations where rectangular spars will go out on the end ribs are also removed. Finally the spars are glued into their respective locations as shown in Figure 3.16.

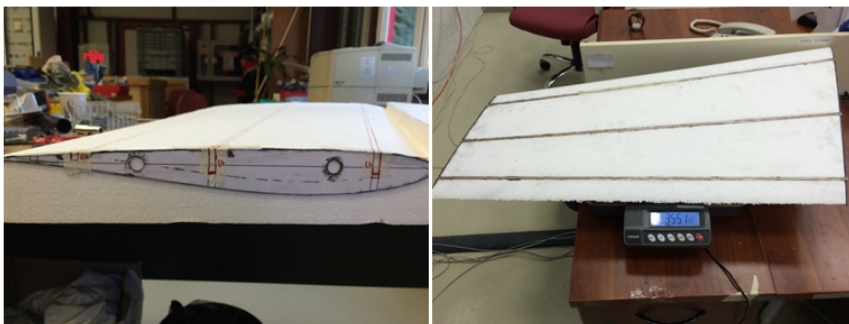


Figure 3.16: Integration of rectangular spars into the part

Wing Piece 1 has two spars to be integrated on both end ribs. The root side integration is similar to that of Wing Piece 2, but tip side spars are buried in to the part. Using the similar method in integration of connection spars to Wing Piece 2, guidelines are drawn; tunnels are drilled using holes on the end ribs as guides. 16 mm spars are glued and integrated into the part on root end side and 10 mm spars are glued and buried on tip side. This is shown in Figure 3.17.

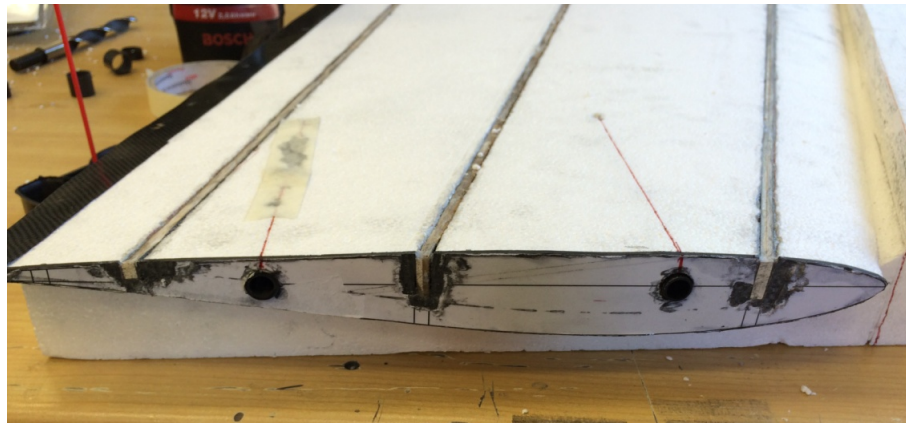


Figure 3.17: Burying of the 10 mm spars into Wing Piece 1

The part is left for a day to cure completely. It is checked for any excess parts and is trimmed by Dremel if there are any. These steps are then repeated for the other Wing Piece 1.

When both Piece 1 and Piece 2 are cured, two pieces are connected to see if they are easy to assemble, to check their continuity in spars, leading and trailing edges and fitting as shown in Figure 3.18.

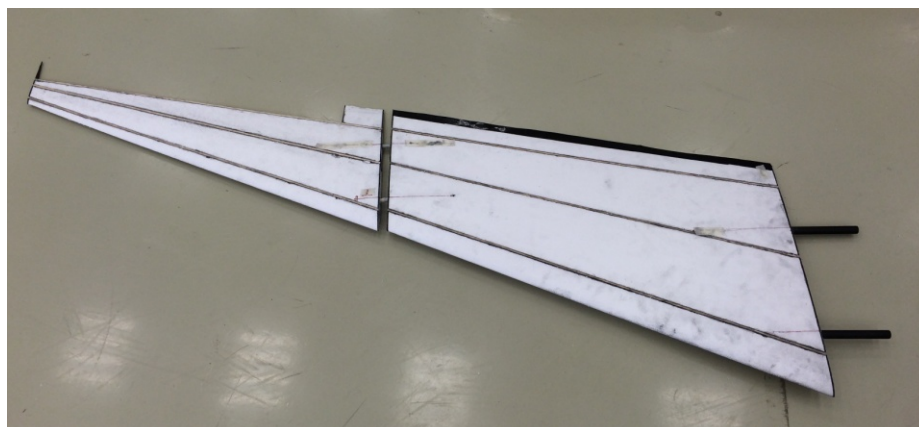


Figure 3.18: Checking the fitting of two pieces together

If there are any problems in the fitting, the connection spars are slightly trimmed using sand paper to ease the insertion.

3.2.4 INTEGRATION TO FUSELAGE

Front side of the fuselage is marked and trimmed to blend the wings. Reference lines for end ribs are drawn on the fuselage for easy gluing of the end ribs as shown in Figure 3.19.

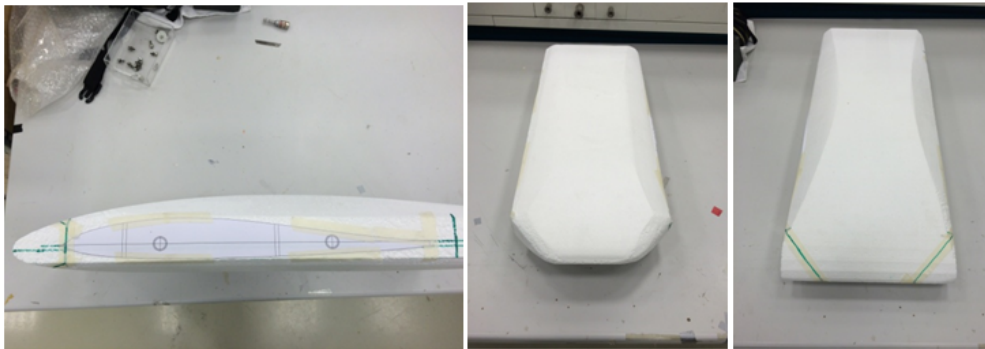


Figure 3.19: Trimming of fuselage leading edge for blending the shape to wings

Using the reference lines drawn, end ribs are glued on both sides of the fuselage. The part is left for half an hour for the glue to be cured. After that, tunnel is opened with long 10 mm drill bit from one side to another using holes on the end ribs as guides. 18 mm spars are glued and pushed through the hole and end ribs. These steps are shown in Figure 3.20.



Figure 3.20: Gluing of end ribs to the fuselage and integration of main spars

After the glue is cured, the excess of the spars are trimmed by Dremel to level with the end ribs. Wing Piece 1 parts are assembled to the fuselage to check the fitting of connection spars into each other and end ribs onto each other. This step is shown in Figure 3.21.



Figure 3.21: Checking the fitting of connection spars of Wing Piece 1 to fuselage

The rear side of the fuselage is trimmed on both edges to make a smooth transition to the motor mount area. The motor mount area as drawn by guidelines and it is cut out using Styrofoam blade. The walls of the motor mount area cut out from 1.5 mm Carbon fiber plate and glued one by one to each side of the motor mount area as shown in Figure 3.22.

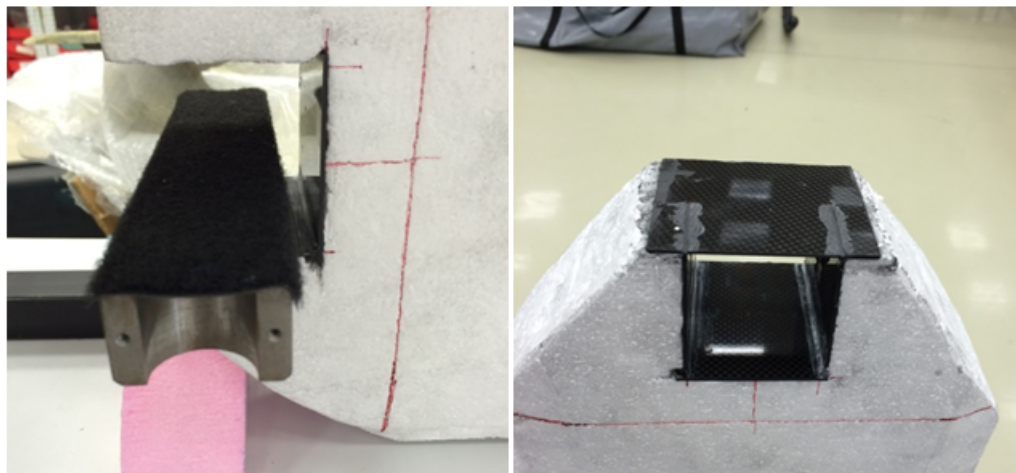


Figure 3.22: Manufacturing of engine mount area

The Carbon fiber plates are glued to each other where they intersect by strong adhesive. The strength of this area is important as it will need to withstand high torques

especially when the motor starts or brakes to a stop. The metal mount piece for the AXI motor is glued on to the end plate and bolt holes on it are drilled as shown in Figure 3.23.

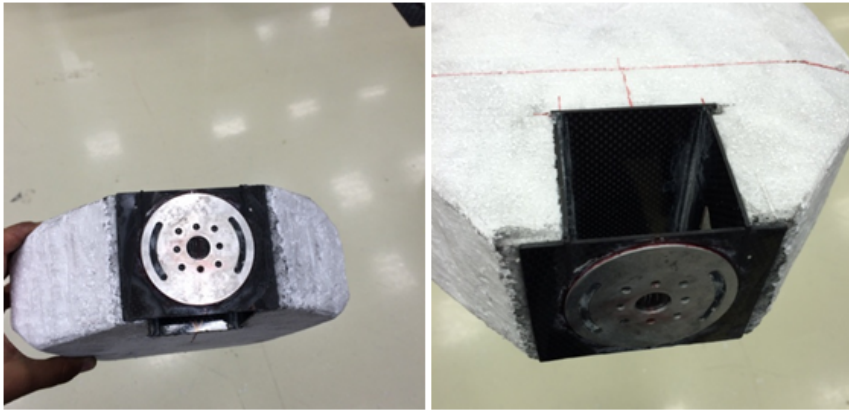


Figure 3.23: Metal motor mount piece assembly

After this, guidelines for rooms to be made inside the fuselage are drawn on the fuselage. The spar locations are also drawn to avoid getting near to these elements while the foam is extracted to make rooms. By the help of these guidelines, three rooms inside the fuselage are opened as shown in Figure 3.24.

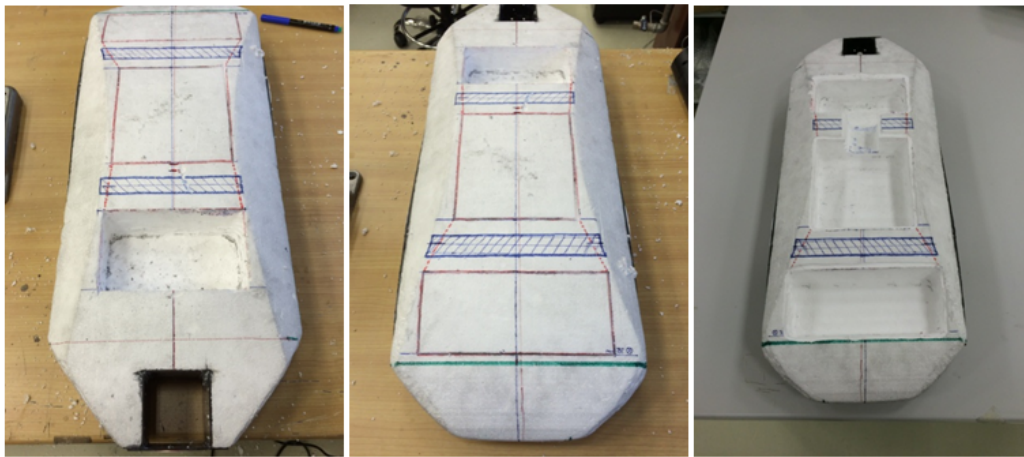


Figure 3.24: Drawing guidelines for rooms and formation of these rooms inside fuselage

Using upper and lower surface molds of the fuselage as molds for composite manufacturing, two composite plates are manufactured using 1 layer of E-glass fiber and 3 layers of Carbon fiber. Produced composite plates are shown in Figure 3.25.

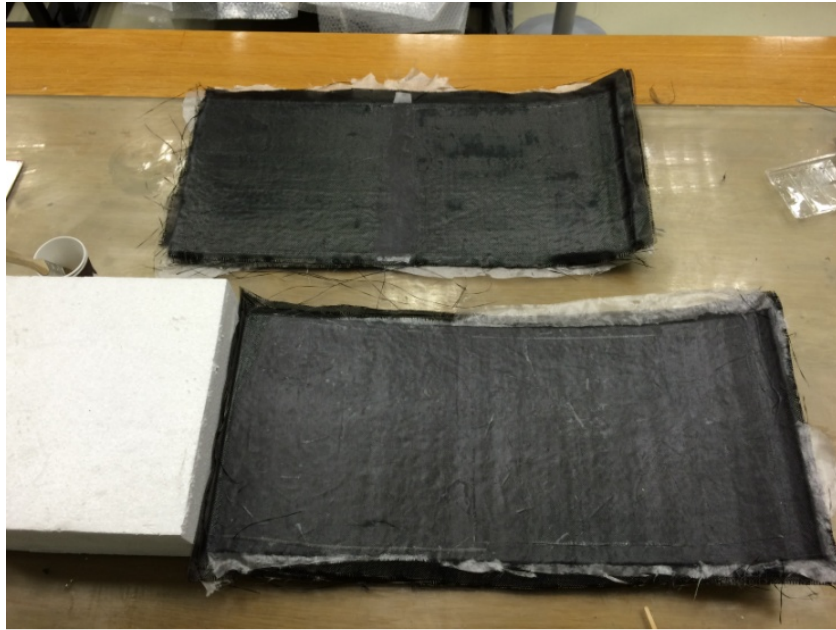


Figure 3.25: Production of composite layers for upper and lower surfaces of the fuselage

The upper composite layer is cut to make covers for the rooms of the fuselage. Lower composite layer is cut to fit the under belly of the fuselage and glued on to create a protective layer for belly landing. Final view of the fuselage is shown in Figure 3.26.

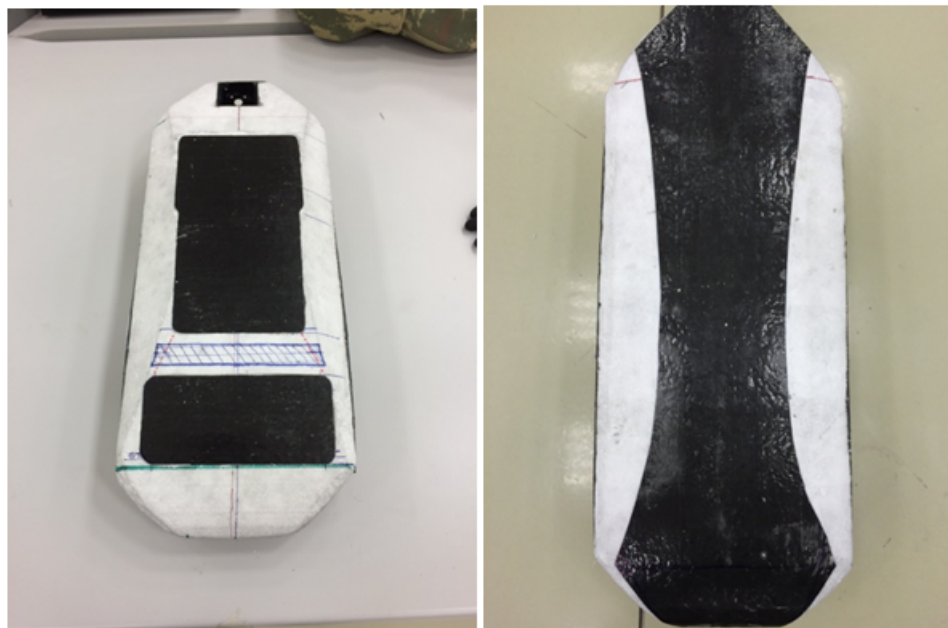


Figure 3.26: Upper and lower surfaces of the manufactured fuselage

The complete structure including control surfaces is weighed and it is found as 1730 gr. This shows that the craftsmanship is fine and the UAV structure is produced within the estimation limits. This is an important issue, as the weight of the UAV structure is actually the most unpredictable in total takeoff weight and producing within the estimation limits almost guarantees that the final weight of the UAV will also be within the weight estimation limits.

3.3 INTEGRATION OF AVIONICS

The avionic requirements of the flying wing design are actually simple. As there is only one control surface (that is the elevons), less number of servos are used than that of a conventional fixed-wing aircraft. This has a side benefit of simplifying the integration and system design of this type of aircraft. The avionics that are assembled to the UAV are as follows:

- AXI 4120/14 motor
- 13"x 8" folding propeller
- Two Volz servos
- Castle Phoenix ICE Lite 75 Amp ESC
- Futaba Receiver
- 8000 mAh 3S Lipo Battery

Battery voltage is chosen according to the designed output of the solar cell grid. After choosing the battery voltage, suitable motor-propeller combinations are done in MotoCalc and the given motor propeller and ESC combination is found. The avionics and their total weight are shown in Figure 3.27.

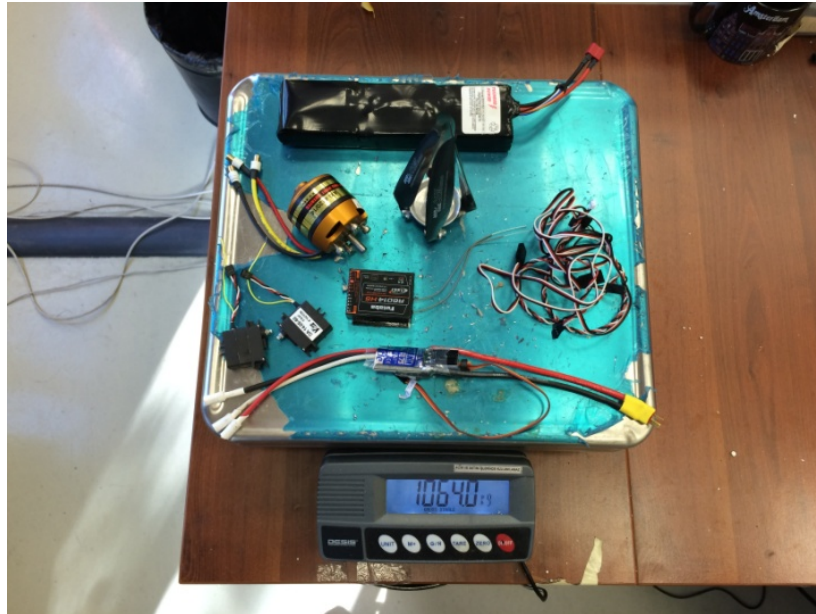


Figure 3.27: Avionics and their weight

The weight of the avionics is slightly over the estimated value of 1000 gr but as the UAV structure was built lighter than expected, it covers for this increase in the avionics.

For the integration firstly, the control surfaces are taped to their location on Wing Piece 2. Aligning to these surfaces, servos are integrated to Wing Piece 2 parts. The place where servo should be is drawn b guidelines. Then this area is trimmed inside using Dremel. The servo is then glued to this servo bay and left for curing, as shown in Figure 3.28.

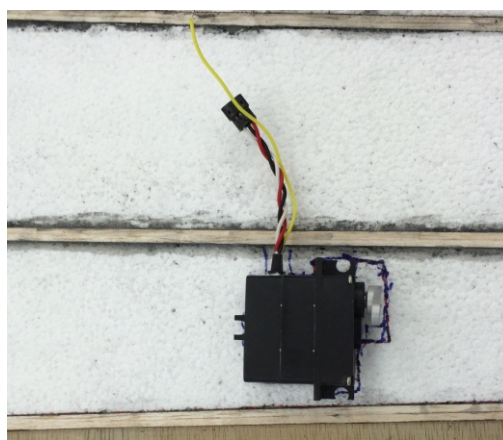


Figure 3.28: Servo integration to Wing Piece 1

Servo cables are taken over the middle spar to the fuselage. After this, motor is assembled to its mount by four M4 bolts and suitable washers. Assembled motor is shown in Figure 3.29.

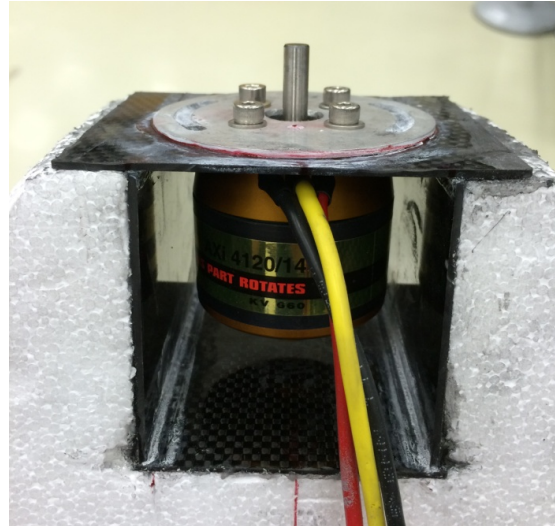


Figure 3.29: Assembly of motor to its mount

After the assembly of motor; ESC, transmitter and battery are assembled inside the fuselage rooms by Velcro tapes. They are not fixed to their positions as they might be required to move to achieve the desired c.g. location. The propeller is fixed to the motor shaft by help of the nut on the centerpiece.

3.4 OVERALL REVIEW AND ASSEMBLY

The servos are attached to the horns on the control surfaces by pushrods. A layer of cured carbon fiber is glued on the trailing edges from both upper and lower sides of the wings to protect them from any damage as these sides are very thin due to the geometry of the profile.

The mixing of aileron and elevator channels on the transmitter is done so that the UAV has elevon (or ailerator) configuration. UAV is fully assembled and system is checked by connecting the battery to ESC. The progress of the UAV from the beginning of the production to the final assembled version is shown in Figure 3.30 and isometric views of the final UAV are shown in Figure 3.31.

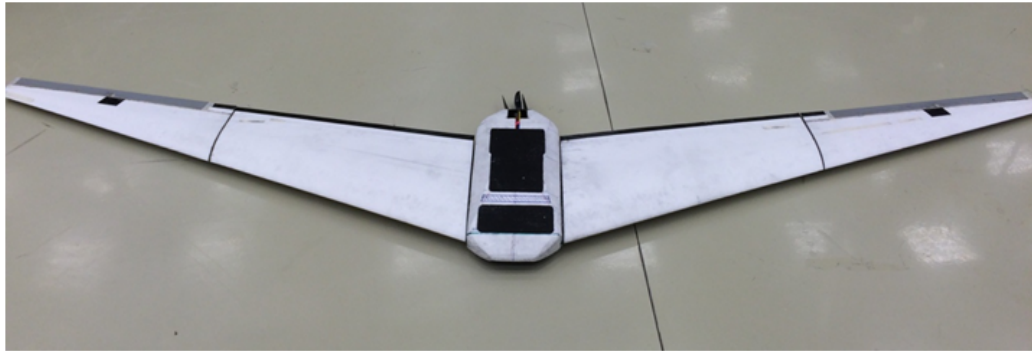
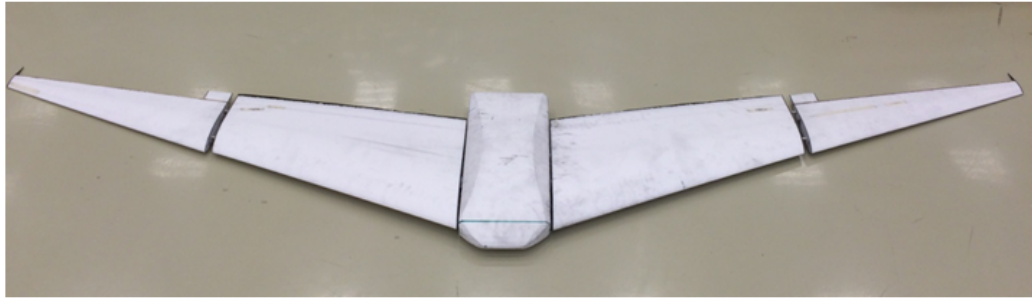
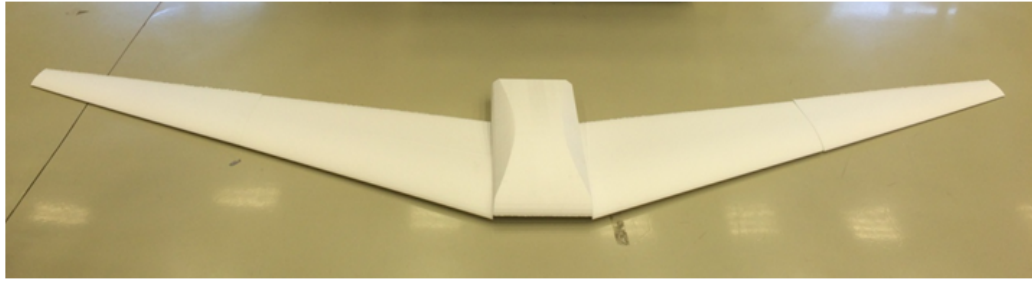


Figure 3.30: Progress of the UAV from the first foam parts to the ready-to-fly final version



Figure 3.31: Isometric views of the UAV

3.5 PRODUCTION OF SOLAR CELLS AND CHARGING CIRCUIT

Each solar cell can give 0.6 V and 2.2 amperes in ideal conditions according to their efficiency. Therefore these cells must be connected in suitable series and parallel combination to meet the power requirements of the UAV and to charge the battery through MPPT unit. Calculations for the number of cells that can fit on the upper surface of each part are done in Excel spreadsheets similar to the one shown in Figure 3.32.

	A	B	C	D	E	F	G	H	I	J	K	L
1	WING PIECE 1											
2												
3												
4		Width (mm)	Length (mm)	Voltage (V)	Current (A)							
5	Large cell	52	156	0,6	2,2							
6	Small cell	19	52	0,6	0,28					30		
7										0		
8		Root (mm)	x1 (mm)	x2 (mm)	x3 (mm)	x4 (mm)	Tip (mm)					
9	Short side	512	478	440	402	365	326			468	97,9%	
10												
11	Long side	820								312	70,9%	
12	Total area	0,338								312	77,6%	
13										312	85,5%	
14										260	79,8%	
15	Number of Cells to be placed (x1)	Short side	Small cell	Large cell								
16	Number of Cells to be placed (x2)	Short side	0	9						0,243		
17	Number of Cells to be placed (x3)	Short side	0	6						0,000		
18	Number of Cells to be placed (x4)	Short side	0	6						0,243		
19	Number of Cells to be placed (tip)	Short side	0	5						72,0%		
20												
21										18	Estimated Average Power (W)	
22										2,2	56,2	
23										39,6		
24												
25										Area (m²)	Power (W)	Output (W/m²)
26												
27										0,008112	1,32	162,7
28										0,000988	0,168	170,0
29												
30												

PANEL DİZİLİMİ	SONUÇ
Seri	Cell orientation and number
Paralel	Covering percentage status
30	1
Large cell	
	OK
	CHECK

Figure 3.32: Calculations done for solar cell placement over Wing Piece 1

Polycrystalline Silicon solar cells are very fragile and they require extreme care and craftsmanship during their assembly. Therefore in order to ease the production only large panels will be used to assemble the solar cell grid. As shown in Figure 47, the solar cells are best connected in 15 series groups, leading to 9 V and 2.2 Amperes, which is 19.8 W per group. Each Wing Piece 1 can support 2 of these groups, each Wing Piece 2 can support 1 and Fuselage can also support 1. Therefore in total 7 groups of 15 solar cells can be connected on the UAV. The calculations are made so that 6 of these groups (total of both wings) will be connected in 2 series and 3 parallel configuration, giving out 18 V and 6.6 Amperes, a total of 118.8 W. Remaining 1 group (which is on the fuselage) will supply payload and communications with 9 V and 2.2 Amperes, a total of 19.8 W. Overall ideal total power estimation is 138.6 W. According to these calculations, to manufacture the cell groups' templates for the upper surfaces of each part of the UAV are formed by laying paper on the upper surface molds of each part as shown in Figure 3.33.

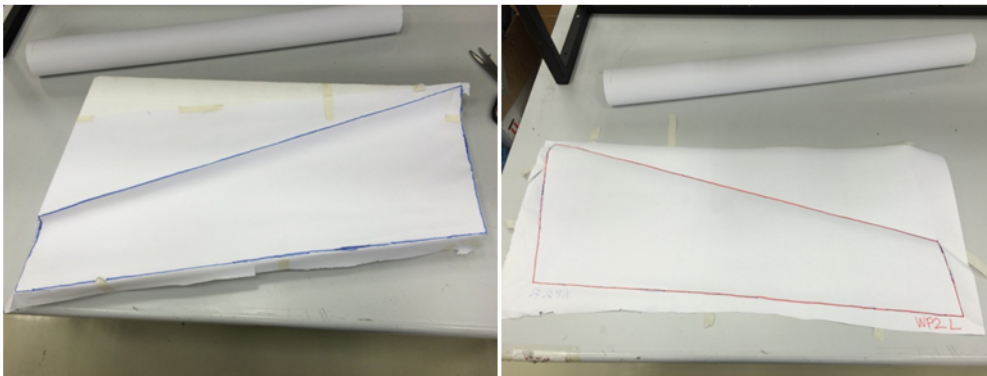


Figure 3.33: Making templates from the upper surface molds of each part

The templates are then cut out and used to form boundaries on a stiff wooden board to represent the surface area of each part. These boundaries help placing panels more efficiently. Boundaries on the wooden board are shown in Figure 3.34.

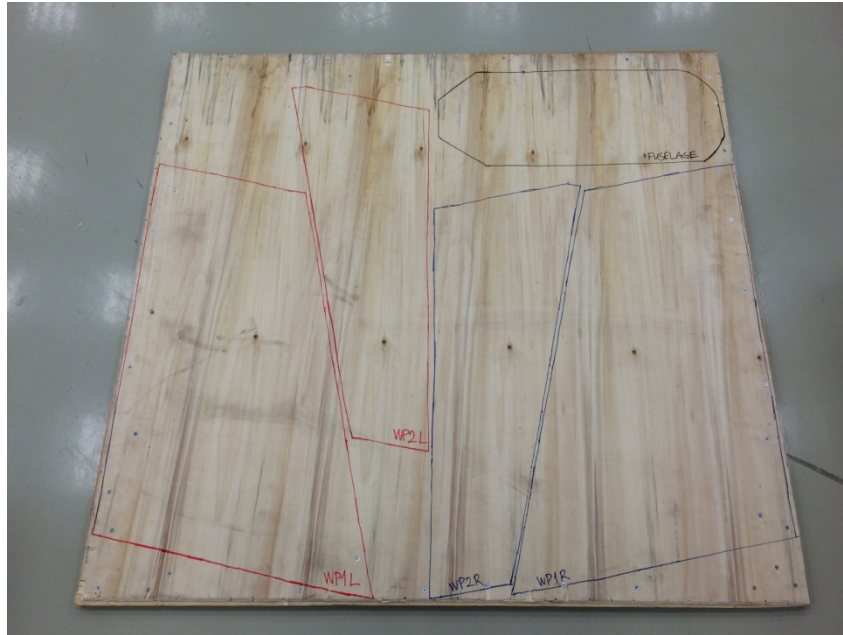


Figure 3.34: Making templates from the upper surface molds of each part

The cells, soldering iron and solder are prepared and solar cells are very carefully and slowly soldered to each other in series one by one as shown in Figure 3.35.

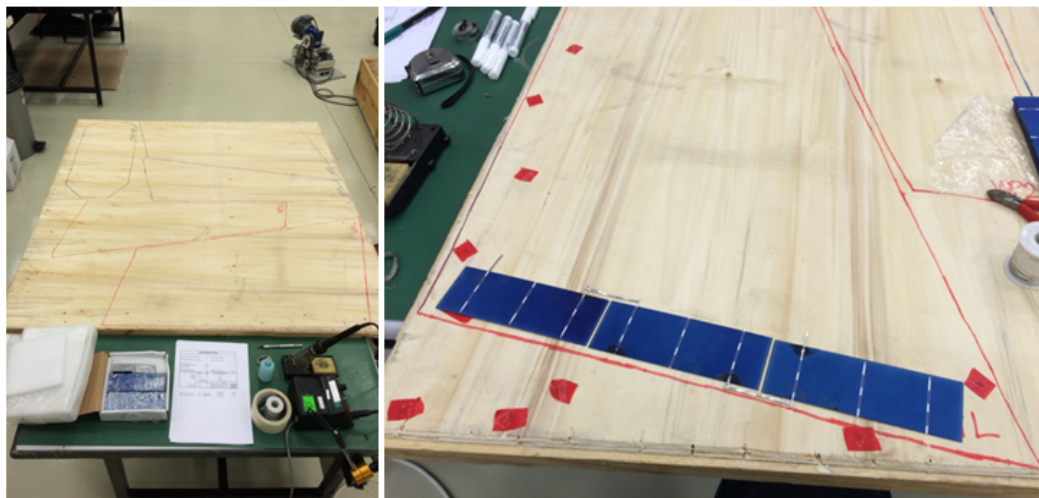


Figure 3.35: Soldering the cells in series

90 cells were successfully soldered 30 cells in series and 3 in parallel. As the cells to supply energy to the motor were complete, it is decided that it is enough to be used in ground testing and to verify the calculations. The cells on the fuselage will be soldered and assembled to the UAV after the ground tests and maiden flight phases are

complete. The charging system is connected to these 90 solar cells in ground testing part in Chapter 4. Solar cell group is shown in Figure 3.36.

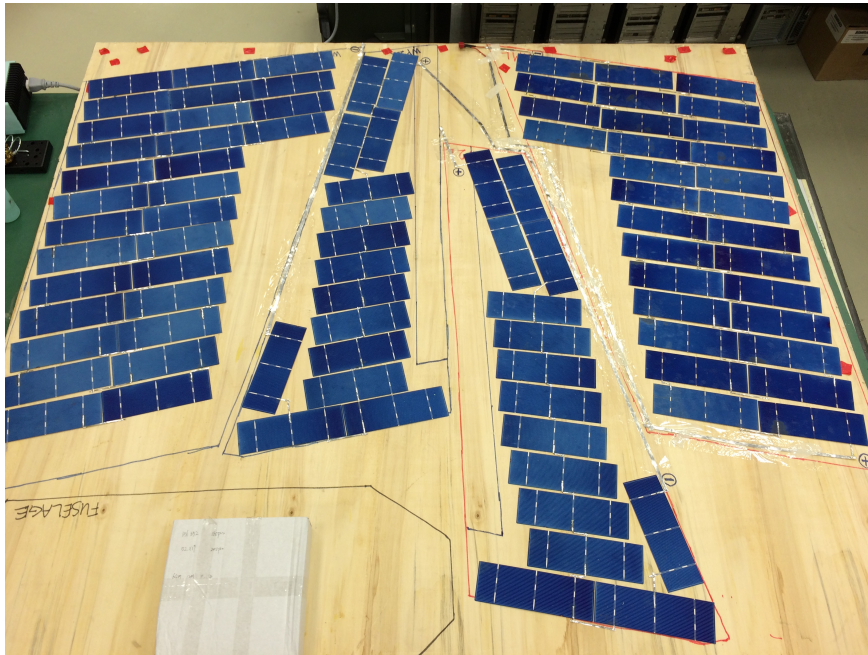


Figure 3.36: 90 solar cell group that will be tested and will be part of the solar cell grid on the UAV

CHAPTER 4

GROUND AND FINAL FLIGHT TESTING

4.1 GROUND TESTS

Ground tests were conducted before the maiden flight of the UAV in order to see if the UAV is ready for further flight tests. These tests focus on measurement of power requirements and power available by the propulsion unit and verification of the solar irradiation estimations and solar power collection calculations done depending on the number of the solar cells placed on the UAV.

Ground tests consist of two parts:

- *Motor Thrust Test*; to observe the full thrust and power available by the propeller-motor-battery combination and the power requirement of the motor.
- *Solar Cell Power Test* ; to test if the 90-cell group can provide the estimated power or not under load.

First ground test was conducted by using a simple thrust measuring setup and live feed of motor voltage, current and power. The setup consists of AXI 4120/14 motor, 13"x8" propeller and 3S 8000 mAh battery, which is the same setup as assembled on the UAV. The data is collected both by the ESC and a data recorder. The setup for this first test is shown in Figure 4.1.



Figure 4.1: Motor Thrust Test setup

Using this setup, current, voltage, power and corresponding thrust measurements were performed for several thrust settings. One example is shown in Figure 4.2.

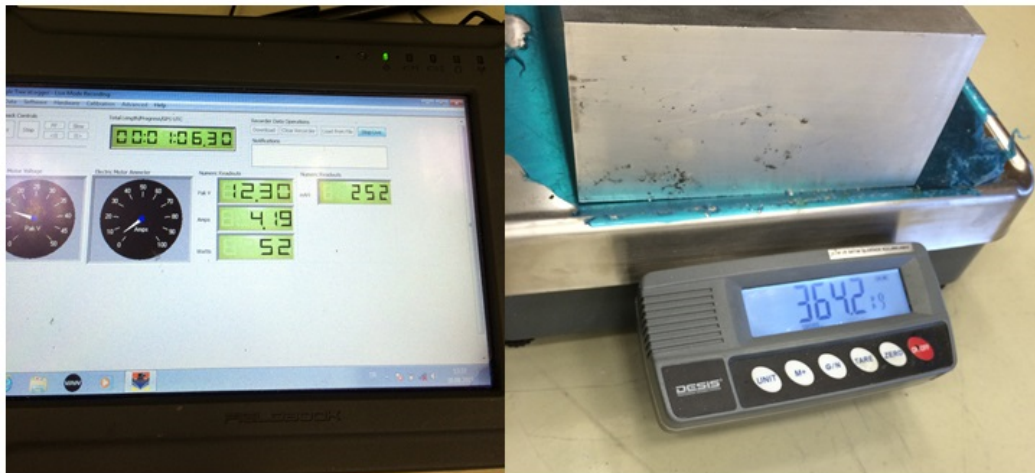


Figure 4.2: Current, voltage and power readings at required thrust for cruise, as an example

The data collected by ESC during the test is shown graphically in Figure 4.3.

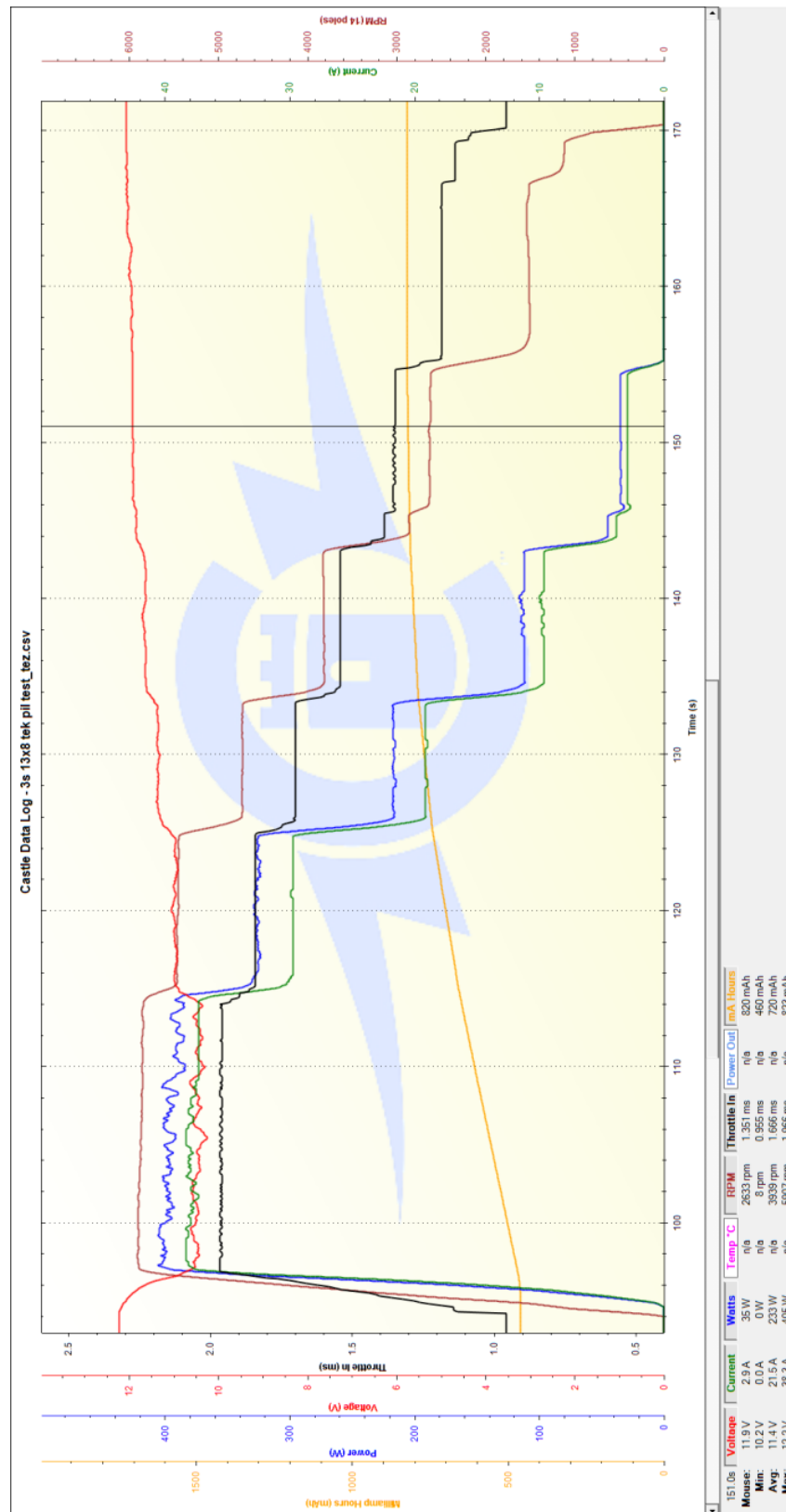


Figure 4.3: ESC Data of the Motor Thrust Test

When the data from the ESC and the thrust values recorded are combined the graph in Figure 4.4 is obtained.

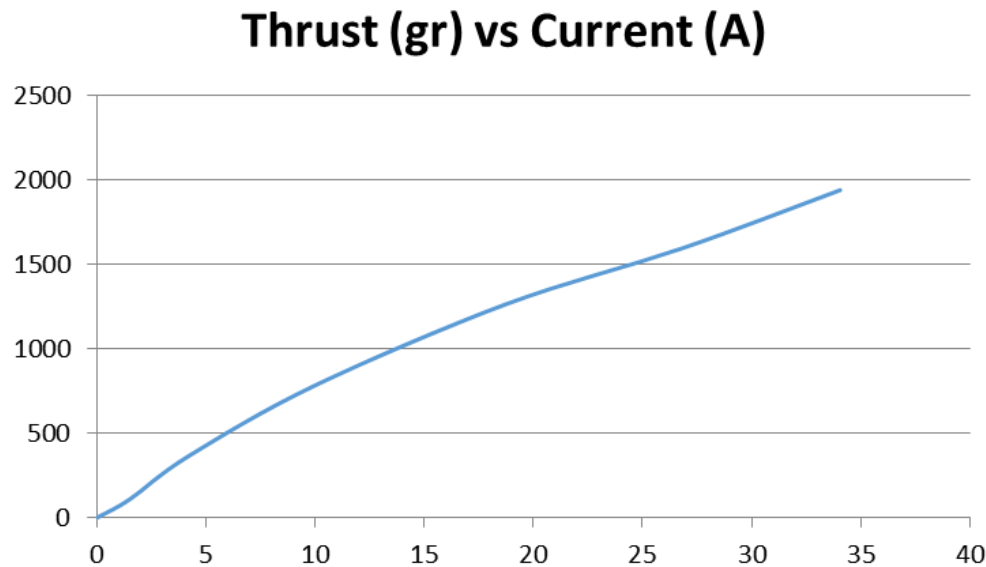


Figure 4.4: Current vs. Thrust graph of the motor test

It can be seen from these figures that, full thrust is 1941 grams at 34 Amperes and 400 W. This is the maximum power required by this motor-propeller setup. For cruise conditions, around 4 Amperes and 46 W, thrust delivered is 348 grams which is consistent with the drag calculations. This test showed that the motor propeller setup matches the estimations that are made during conceptual design phase and performance analysis.

After this test, solar cell power test was conducted. This time, the thrust test setup was not used as current vs. thrust graph was already obtained, the thrust can be calculated by looking at the current. The setup for this test included 90-solar cell group connected to MPPT, to the battery and to same ESC, motor and propeller. Suitable Schottky diodes were soldered at the positive pole of each 30-cell group of solar cells so that if any of the solar cell groups supply lower voltage (due to shading etc.) than others the diode will block the current and prevent that group to act as load and drain power. The soldered diodes are shown in Figure 4.5.

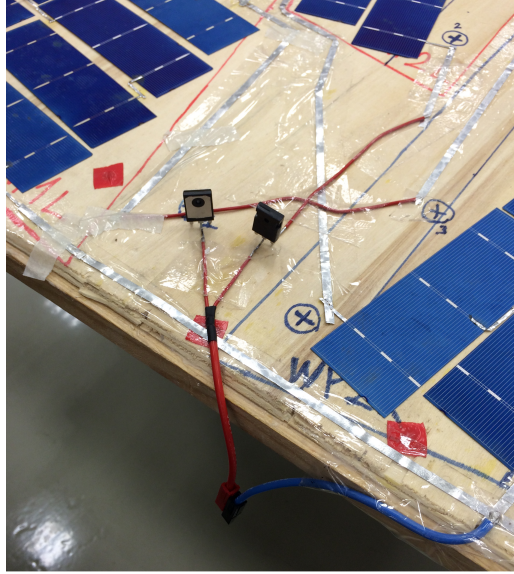


Figure 4.5: Schottky diodes (black) soldered at the positive pole of the solar cell groups

After the setup of solar cells was ready the test was conducted on November 22nd. The sky was not perfectly clear, some thin clouds were scattering the sun rays. The clearness index was calculated as 0.55 for that day. A view of the test day at the test hours is given in Figure 4.6.



Figure 4.6: A view of the clearness of the sky on the test day

Before the tests begin an estimation of the solar energy collection was made by using Equations (from 2.8 to 2.11) given in 2. The parameters given below were also used

for the test day;

n : day number = November 22nd = 326

δ : Declination = -20.64 (for November 22nd)

ϕ : Latitude of the test area = 40.12

ω : Time of the day converted to degrees (12:00 being 0 and for each hour 15 degrees is added or subtracted) = 10 to 11 am

($\omega_1 = -30$ and $\omega_2 = -15$)

Using all these data, solar energy estimation was found as, $I_{estimated} = 1.201 \times 10^6 J/m^2$.

Converting this value to power per meter square gave $334 W/m^2$. Considering the total area of 90 solar cells with conversion efficiency of 17.6% is $0.73 m^2$ and efficiencies of MPPT, ESC, motor and propeller, the power output estimation was calculated as 35 W. This showed that on the test day, the required power for cruise conditions may not be acquired but still the endurance can be increased as most of the power required can be covered by the solar cells.

After the estimation, 90-cell group was first connected directly to propulsion unit to see whether they can produce enough estimated power to turn the propeller at sufficient RPM. The test setup and the voltage reading of the solar cells are given in Figure 4.7.

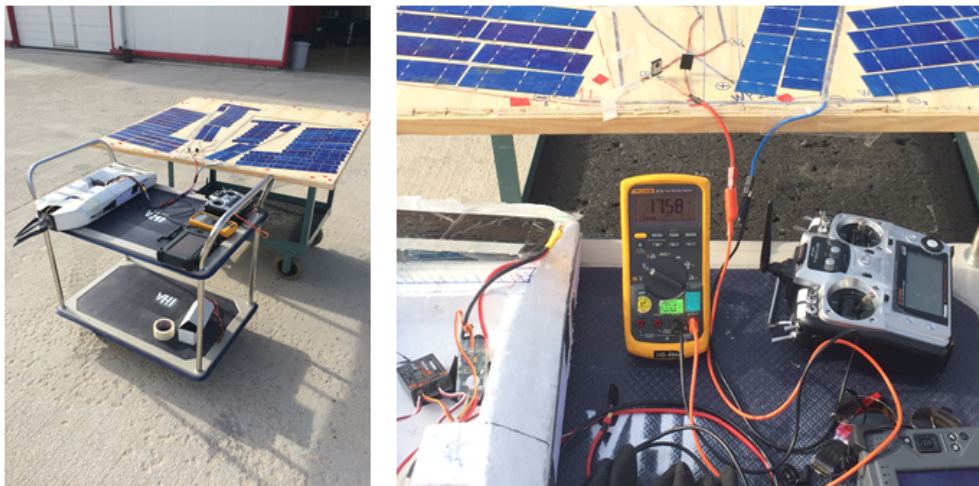


Figure 4.7: Test setup (left) and the voltage reading from the 90-cell group (right)

It was measured that solar cells can turn the propeller up to 2000 RPM and keep it steady at that level. Considering the thrust required for cruise is 350 grams and RPM at that thrust is around 2600 and thrust is roughly proportional to square of RPM;

thrust is calculated to be 207 grams. This corresponds to 26 W of power delivered by solar cells only. With the addition of MPPT circuit, it can be estimated that the power output of the solar cells can be increased by 30% in average, leading to a value of 34 W. This value is consistent with the power output estimation done in previous paragraph by solar irradiation calculations. After the completion of the first part of the test, the actual test of power consumption with and without solar cells was done. The test procedure is to measure the consumption from the battery by simulating a short flight of the UAV on ground. The simulation of the flight will take 15 minutes in which full throttle command will be given for the first 20 seconds to simulate take-off and climb and for the rest of the test cruise throttle command will be given to motor. This test was done for two cases;

- The setup with the battery only
- The setup with battery, MPPT and solar cells

The test setups of two cases are shown in Figure 4.8 and in Figure 4.9.



Figure 4.8: Test setup with the battery only

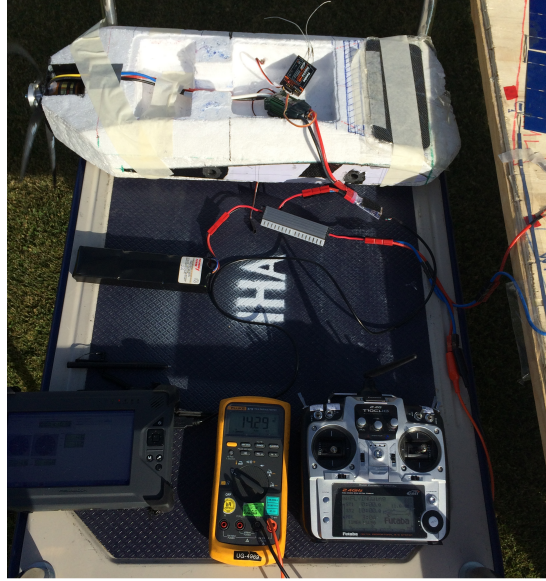


Figure 4.9: Test setup with battery, MPPT and solar cells

After each case, the battery was removed and charged. The recharged value to the battery in mAh was noted. The resulting consumptions from the battery for each case are shown in Figure 4.10.

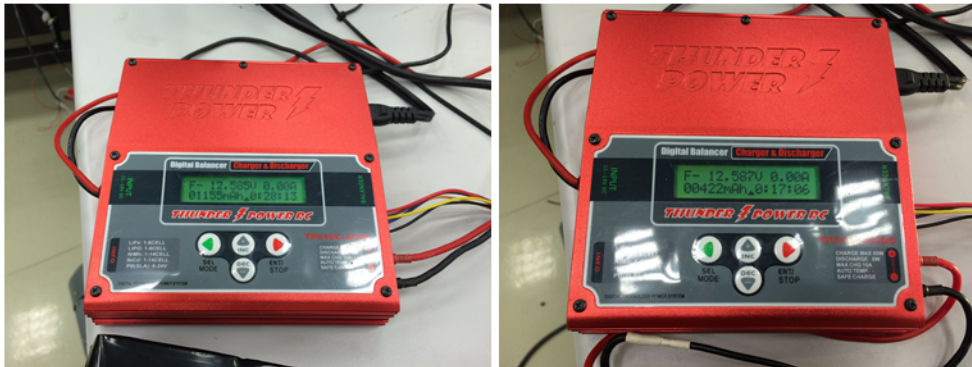


Figure 4.10: Consumption from the battery for only battery case (left) and consumption from the battery for battery, MPPT and solar cells case

It was expected that the consumption from the battery in the second case will be lower but not zero as the estimated power supplied by solar cells is less than the required power for cruise on the day of the test. This difference in consumptions shows that the endurance of the UAV is greatly increased. In order to calculate the exact increase in the endurance the ESC data graphs from both tests are examined. These graphs are given in Figure 4.11 and in Figure 4.12.

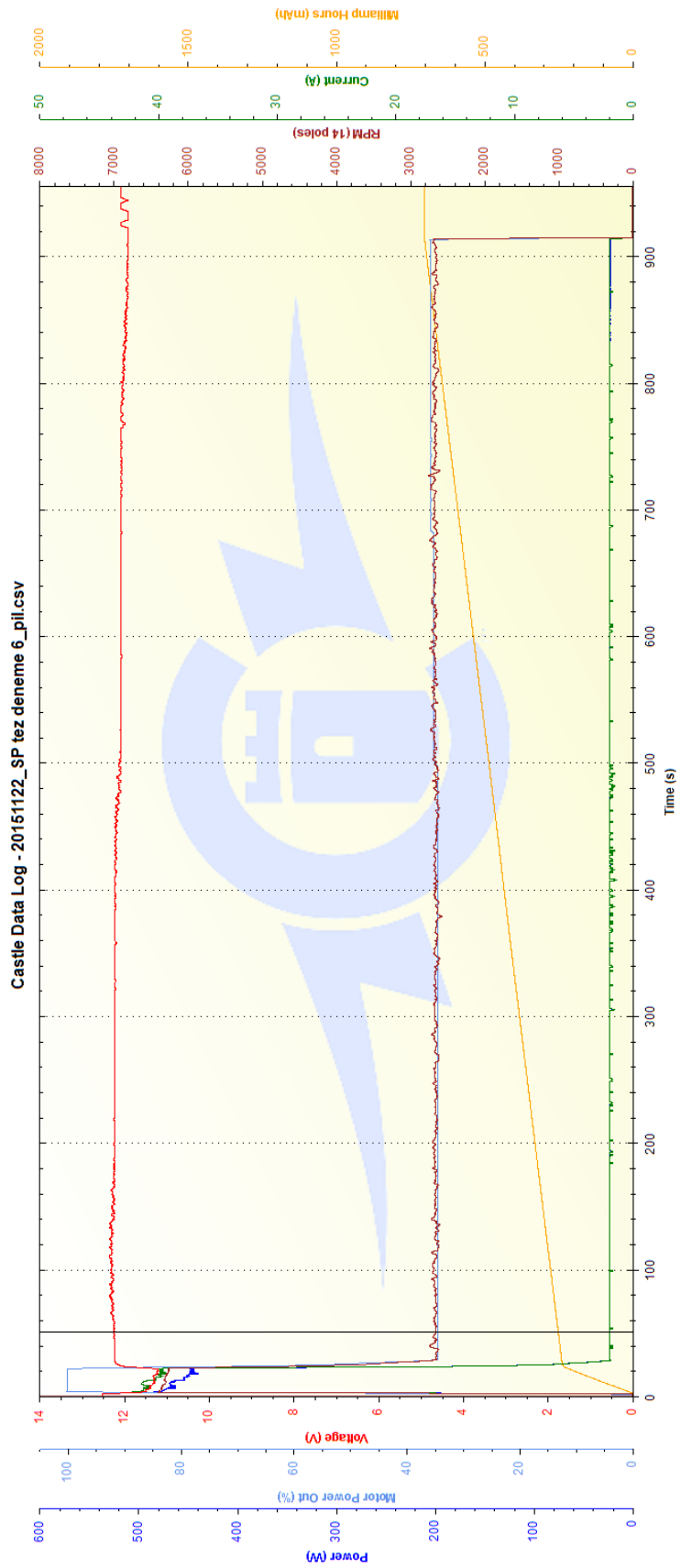


Figure 4.11: ESC data graph of the test with the battery only

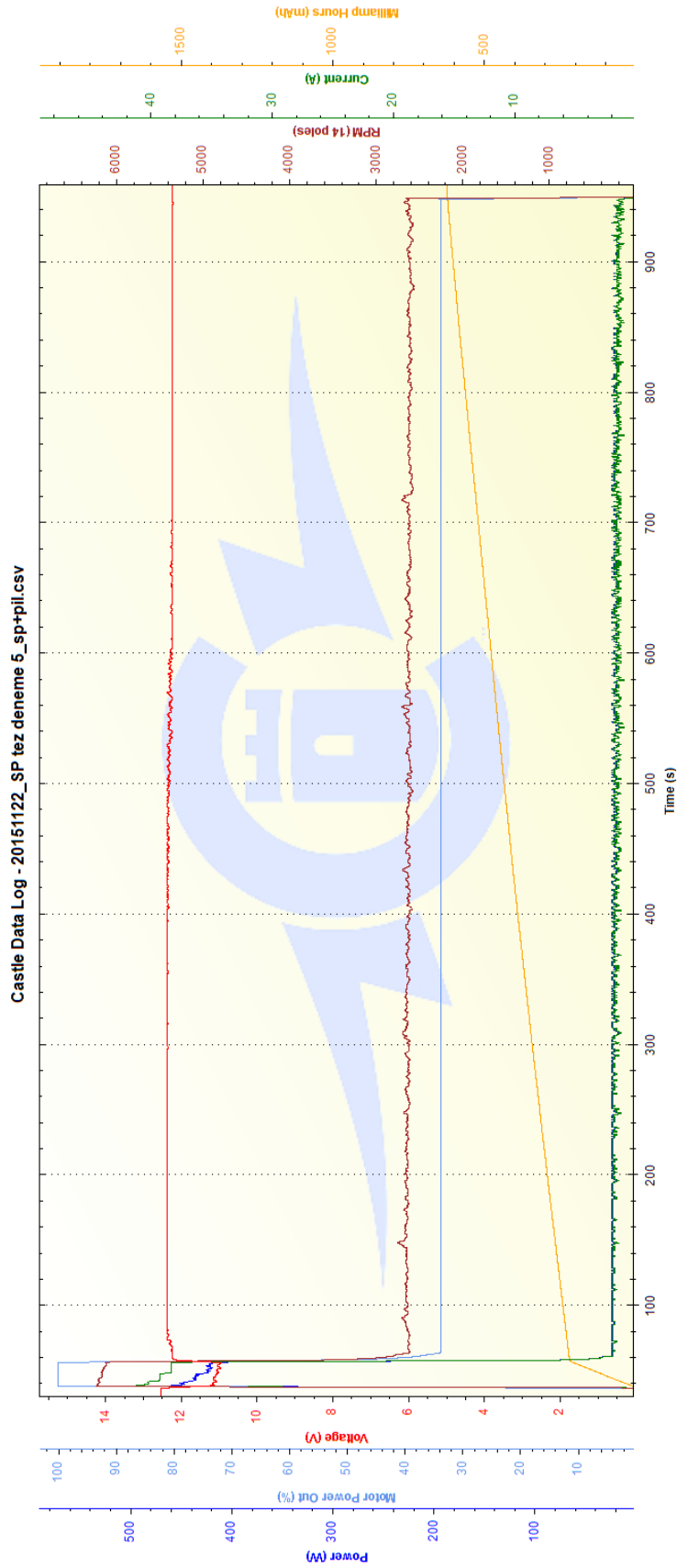


Figure 4.12: ESC data graph of the test with battery, MPPT and solar cells

It is measured from the graphs that during take-off phase the consumption is 220 mAh. Subtracting this value from total consumption of each case, consumption values for cruise phases of each case are obtained;

- Cruise phase consumption from the battery for the first case:

$$1155 - 220 = 935mAh \quad (4.1)$$

- Cruise phase consumption from the battery for the second case:

$$422 - 220 = 202mAh \quad (4.2)$$

The remaining battery capacity for cruise phase is 7780 mAh, when take-off phase is subtracted from total capacity of 8000 mAh. As the consumption values calculated above are for 14 minutes 40 seconds of cruise, estimated endurance for both cases can be calculated as follows:

- Estimated endurance for battery only case:

$$\frac{7780}{935} \times 14.67 = 122minutes \approx 2hours \quad (4.3)$$

- Estimated endurance for battery, MPPT and solar cells case (actual setup):

$$\frac{7780}{202} \times 14.67 = 565minutes \approx 9.4hours \quad (4.4)$$

From these results, it can be concluded that even though the required power for cruise cannot be obtained from the solar cells (for example on winter days), as the area covered by the solar cells is large, it increases the endurance of the UAV dramatically for flights below cloud levels. Considering the total weight of the solar cell system on this UAV is 510 grams, no battery replacement at the same weight can give this increase in the endurance.

As conclusion, all ground tests are completed successfully. Especially for solar system tests, working in non-ideal conditions and still obtaining satisfactory results increased the confidence in the design.

4.2 MAIDEN FLIGHT TEST

Maiden flight test is to be conducted after the ground tests to verify the estimations and the overall system stability in means of power requirements. This test is a short radio-controlled (RC) flight to verify the stability of the design and to observe the overall flight characteristics of the UAV and its structural behavior under flight conditions. ESC data during flight will also be collected but as it will be a RC flight, the consumption values may not be as low as calculated for the autopilot case. The test will be conducted with the manufactured UAV, without the solar panels nor the autopilot. The weight of the UAV for this configuration will be increased to 4000 grams by adding dummy weights, therefore the UAV will be tested under its normal mission conditions.

First flight test was conducted under zero wind condition and on a clear day. The UAV was fully assembled including its winglets as shown in Figure 4.13.



Figure 4.13: Fully assembled UAV prototype ready for RC maiden flight

The UAV was launched by hand and full throttle was given right after launch, as its normal hand-launch procedure. The UAV could not take off and crash-landed towards its left wing right after full throttle was given, as shown in Figure 4.14.

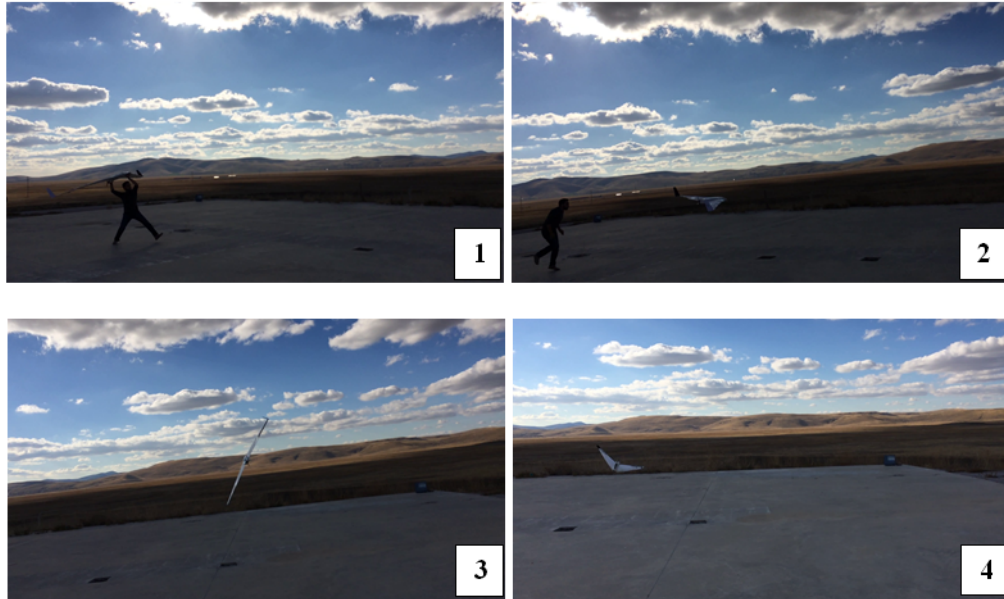


Figure 4.14: Hand-launch of the UAV (1); giving full throttle command (2); UAV rolls left uncontrollably (3); UAV crash-lands on its left side

The test was unsuccessful. However the UAV structure was almost undamaged. After the videos were examined, the reasons for the unsuccessful take-off were found as follows:

- The motor torque at the start was not balanced, as there was no incidence angle given to the motor shaft to counteract the torque of the motor.
- The wings are found to be not rigid enough, which may lead to decrease in the effectiveness of the control surfaces as observed during hand launch. Therefore the structure of the UAV needed further support to increase the stiffness and rigidity of the UAV and reduce its elastic behaviour.

In the scope of these outcomes, firstly an angle of incidence of 2 degrees was given to the motor shaft by adding washers to one side between motor mount and the motor, to take care of the encountered torque issue during start. Secondly, one layer of $93\text{gr}/\text{m}^2$ Carbon fiber and one layer of $25\text{gr}/\text{m}^2$ E-glass fiber was applied with resin to the lower side of left and right Wing Piece 2, as shown in Figure 4.15. The root spars of the wings are also supported from the lower side by addition of carbon fiber layer and adhesive as shown in Figure 4.16.

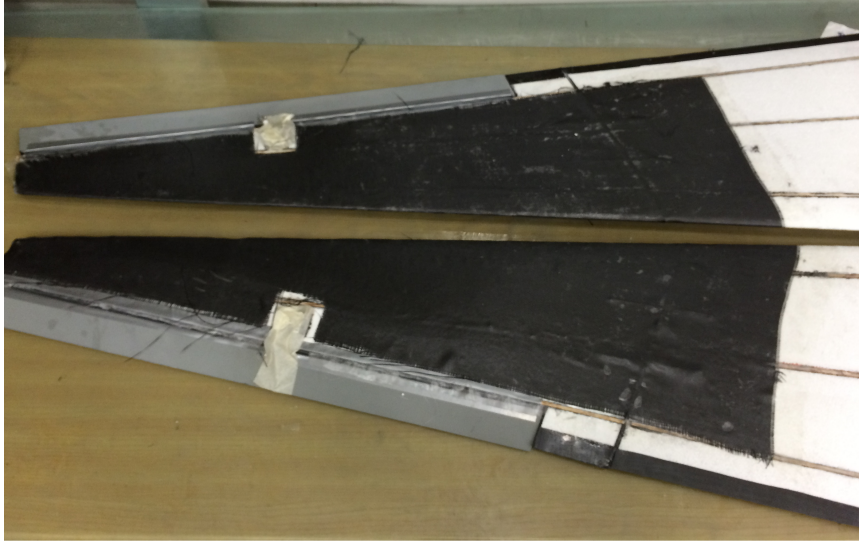


Figure 4.15: Application of Carbon fiber and E-glass fiber to the lower side of Wing Piece 2 of both wings



Figure 4.16: Addition of Carbon layer and adhesive to root spars of the wings

These structural enhancements added an extra weight of 80 gr in total to the UAV, but this weight increase is compensated by removal of winglets for the second maiden flight test. The winglets are removed for the initial flight tests for removing the tip weights for a more stable wing structure.

After this review of the overall structure, the second trial for the maiden flight was

done. This time, there was 4 m/s headwind at the test area therefore the UAV took off easily without much of a push during hand-launch, as the stall speed was calculated as 5.2 m/s. The pilot gave full throttle for a couple of seconds as the UAV did not require any more thrust to climb and glide. The hand-launch, take-off and climb are shown in Figure 4.17.

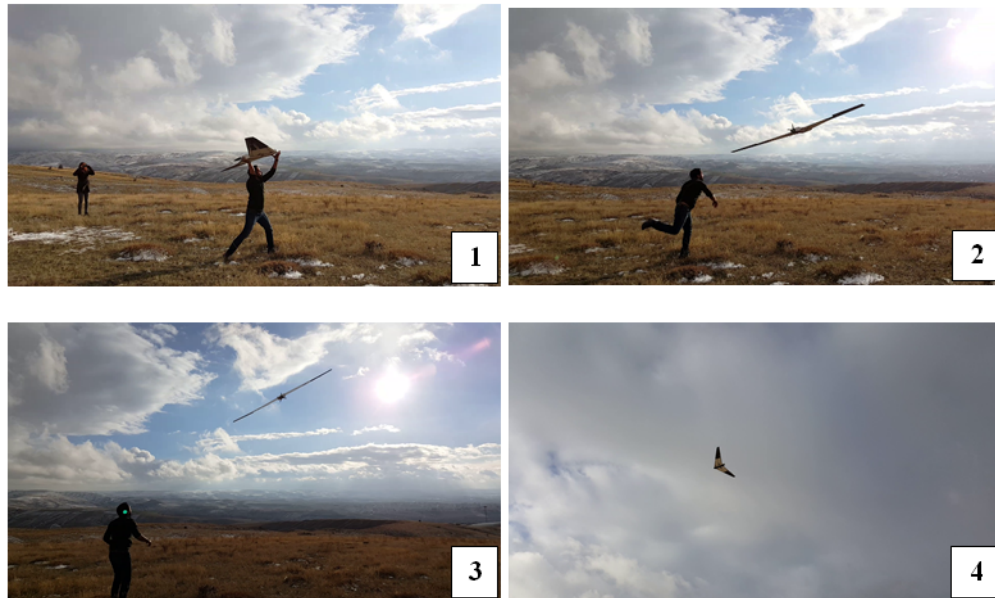


Figure 4.17: Hand-launch (1); take-off (2); climb (3) and flight (4) of the UAV during its maiden flight

The UAV flew successfully for one minute. During the flight the UAV exceeded its design speed limits due to high headwind conditions and a small diving maneuver during approach. Due to this, the structure went into flutter state but went out of the state quickly without any damage to the wing and the fuselage when pilot reduced the flight speed of the aircraft by cutting off the throttle and letting it to glide. This showed that the structure was still elastic at the wing-fuselage connections and needed to be stiffened by adding a third connection spar to the roots of the wings. This is an enhancement that will not affect the outer geometry of the design but increase its rigidity and enhance its reliability for such possible cases. After gliding, the UAV landed safely, as shown in Figure 69. The pilot's comments were that the UAV was stable in its flight envelope and it is easy to fly as a glider, which verified the design and that the produced UAV was flying as it was intended.



Figure 4.18: UAV landed after its maiden flight

As the maiden flight test was successful, it can be concluded that the design is verified and the prototype UAV can be assembled by the assembly of solar cell system on to the UAV skin.

After the maiden flight, assembly of solar cells on to the wings was started. The UAV in its final form can be seen in Figure 4.19.

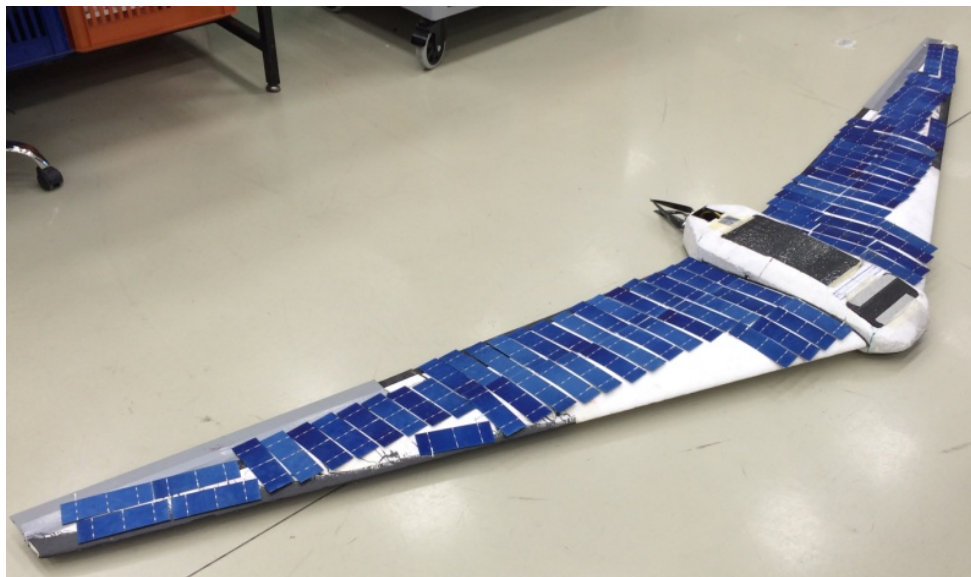


Figure 4.19: The solar powered UAV with solar cells on its wings, before fixing

CHAPTER 5

CONCLUSION

It was aimed at the beginning of this thesis work to design and manufacture a sustainable solar powered mini UAV. To accomplish this and add a different perspective to previously built solar powered aircraft, a flying wing UAV was designed. This choice was done to lower the drag with a better aerodynamic design than conventional aircraft thus, lowering power requirement for flight and increasing the possibility of sustainable flight by solar power. The designed UAV was produced using foam with composite structural elements. After the production of the prototype UAV, it was flown in its maiden test. It was a successful maiden flight and, during the test, the UAV entered a state of flutter due to exceeding speed limits of its flight envelope but went out of the state undamaged. It was unexpected but also was very important to be experienced as this showed that the UAV structure required more stiffness. This was solved with an enhancement to wing-fuselage connection. This experience also showed how important flight testing is, as computer analysis can be done on aircraft over and over again but the design process can never be complete without verifying the aircraft under real flight conditions.

It was also important to produce a sustainable power system to convert solar energy into electrical energy to be used by the UAV. Crystalline Silicon solar cells were used to build such a system along with a MPPT circuit to regulate the output voltage and current for increasing overall conversion efficiency of solar cell grid. With the addition of a reservoir battery, regulated and non-fluctuating power is supplied to all systems on board while this battery is charged by the solar cells. This system was tailored-fit for the total wing and fuselage upper area of this UAV and its output performance was successfully tested by ground tests. Combining these two important

aspects, the designed UAV and the designed solar power system, in this thesis resulted in a mini flying-wing UAV with solar cells integrated to its power system and this thesis work reached its goal.

Therefore as a conclusion for this thesis work, it can be said that it is possible to build a sustainable solar powered system integrated onto a system of a mini UAV. The design of prototype UAV manufactured in the scope of this work is verified by flight tests; therefore it is certain that it can carry the given amount of solar cells within its flight limits. Along with the verification from the ground tests, it can use collected solar power, at least to, increase its endurance up to 9 hours along with supplying power for communication and payload needs. This estimation on the endurance of the UAV can be verified with additional flight tests including the autopilot, which is beyond the scope of this work. Looking at the results obtained from solar cell power tests done in winter time, it is possible to estimate that the UAV can stay aloft as long as it sees the Sun during summer time, increasing its endurance further to 13-14 hours on average, including its battery only flight time after sunset.

It is important to emphasize that this significant increase in its endurance is sufficient to make this a sustainable solar powered UAV and the flying wing design is possible. Approaching “the use of limited power on solar powered aircraft” problem from the perspective of lowering the drag by changing the conventional design to flying wing design, as done in this thesis work, seems to be a successful decision. This approach will also be much more convenient as the solar cell technology advances and more efficient solar energy collection configurations will be available.

For the future work, autonomous flight tests will be conducted for endurance and system verification within the mission requirements of this UAV. Furthermore, type of the solar panels can be changed to more flexible solar panels to ease the solar cell grid production as polycrystalline Silicon cells are very fragile and need extreme care and craftsmanship to work with. Flexible solar panels, like the ones by Alta Devices, with similar efficiencies can be used for this design.

REFERENCES

- [1] Guclu Ozcan; Nafiz Alemdaroglu. Solar irradiation estimation on a solar powered uav. *International Conference on Unmanned Aircraft Systems (ICUAS), Denver, USA.*, 2015.
- [2] John D. Anderson. *Aircraft Performance and Design*. McGraw-Hill, 1999.
- [3] Martin Hepperle. Basic design of flying wing models. <http://www.mh-aerotools.de/airfoils/flywing1.htm>.
- [4] Andre Noth. History of solar flight. http://www.asl.ethz.ch/research/asl/skysailor/History_of_Solar_Flight.pdf.
- [5] Andre Noth. *Design of Solar Powered Airplanes for Continuous Flight*. ETH Zurich, 2008.
- [6] NREL. National center of photovoltaics. <http://www.nrel.gov/ncpv/>.
- [7] U.S. Department of Energy. The history of solar. https://www1.eere.energy.gov/solar/pdfs/solar_timeline.pdf, p.2.
- [8] U.S. Department of Energy. The history of solar. https://www1.eere.energy.gov/solar/pdfs/solar_timeline.pdf, p.3.
- [9] U.S. Department of Energy. The history of solar. https://www1.eere.energy.gov/solar/pdfs/solar_timeline.pdf, p.4.
- [10] Will Reece. The history of solar power. https://www.experience.com/alumnus/article?channel_id=energy_utilities&source_page=additional_articles&article_id=article_1130427780670.
- [11] Airfoil Tools. Airfoil tools-e186. <http://airfoiltools.com/airfoil/details?airfoil=e186-il>.
- [12] Airfoil Tools. Airfoil tools-mh61. <http://airfoiltools.com/airfoil/details?airfoil=mh61-il>.
- [13] Wikimedia. Wikimedia foundation inc. flying wing. https://en.wikipedia.org/wiki/Flying_wing.

[14] Wikimedia. Wikimedia foundation inc. sunlight. https://en.wikipedia.org/wiki/Sunlight#/media/File:Solar_spectrum_en.svg.